CHARACTERIZATION AND APPLICATION OF UBIQUITIN E3 LIGASE RNF146 WWE DOMAIN

by
Haobo Wang

A thesis submitted to Johns Hopkins University in conformity with the requirements for the degree of Master of Science

Baltimore, Maryland

August, 2016

Abstract

Poly(ADP-ribosyl)ation (PARylation) is a reversible post-translational modification of cellular proteins. The dynamic process of PARylation is balanced through synthesis of poly(ADP-ribose) (PAR) on substrates by PAR polymerases (PARP) and degradation of the polymer by PAR glycohydrolase. Here we report that overexpression of RNF146 and its PAR-binding WWE domain led to an increase in endogenous PAR level in multiple cell lines. Moreover, we showed that the increase in PARylation level was likely due to an increase in the steady-state level of certain PARylated proteins such as PARP5a (Tankyrase 1) and PARP5b (Tankyrase 2). At a single cell level, we observed the formation of PAR/Tankyrase-rich puncta in HeLa cells by overexpressing RNF146 WWE domain. We also demonstrated the PAR induction by RNF146 WWE domain was tightly linked to its affinity for PAR. Mutations in RNF146 WWE domain reducing PAR binding (Q155A, Y143A and R163A) also impaired PAR/TNKS induction level upon overexpression in cells. We illustrated that such a characteristic property of RNF146 WWE domain was not a common feature shared by every member in the mammalian WWE domain family. Lastly, we proposed and explored the idea of engineering RNF146 WWE domain into a molecular tool for artificially augmenting PARylation level in different subcellular compartments.

Acknowledgement

I would like to use this opportunity to express my sincere gratitude to my thesis advisor Dr. Anthony Leung for his mentorship and support, for his patience, motivation and understanding. His guidance helped me push through my research as well as writing of this thesis. I thank my lab colleague Dr. Yoshinari Ando for his mentorship, encouragement and daily support for my research project. I would also like to thank Dr. Michael Matunis for his insightful advice and precious support over the years. In addition, I would like to thank my fellow labmates for creating an enjoyable working environment in lab. Last but not the least, I would like to thank my family, especially my parents, for their continuous support and understanding.

Table of Contents Page Reference

List of Tables

List of Figures

Introduction

ADP-ribosylation

ADP-ribosylation refers to the attachment of ADP-ribose units onto target proteins. It was first identified as a nucleic acid product resulting from addition of nicotinamide mononucleotide in chicken liver nuclear extracts in the absence of the other nucleotide triphosphates (Chambon and Mandel, 1963). Further analysis discovered the chemical structures of this product as a polymer of ADP-ribose (Chambon et al., 1966). The post-translational modification can exist in two forms: poly(ADP-ribosy)lation (PARylation) and mono(ADP-ribosy)lation (MARylation). As their names indicate, MARylation is a process attaching single ADP-ribose (ADPr) units onto proteins, whereas PARylation allows attachment of additional ADPr units to form a polymer chain on a target protein. The chain can be elongating either in a linear or branched fashion up to hundreds of units in length. Both in the linear portions and at branched points of PAR chains, ADPr units are covalently connected by α(1-2) ribose–ribose bonds (Miwa et al., 1981). However, the exact significance of differences in PAR chain structures is still unclear. After the discovery of ADP-ribosylation, enzymes that catalyze the reactions were also identified over the years and commonly known as poly(ADP-ribose) polymerase (PARP). To date, 17 PARPs have been discovered in mammalian cells (Vyas et al., 2014). In general, PARPs can transfer ADPr from NAD^+ to the specific target residues of a protein. Recent studies have indicated that 4 out of 17 mammalian PARPs, namely, PARP1, PARP2, PARP 5a, and PARP5b (also known as Tankyrase 1 and 2, or TNKS 1 & 2), are capable of carrying out PARylation in vitro. On the other hand, both major isoforms of PARP13 as well as PARP9 have been characterized as catalytically

inactive for ADP-ribosylation, whereas the other PARPs are believed to catalyze MARylation in cells (Vyas et al., 2014). Given the fact that some members of the PARP family can only carry out the MARylation process, a new nomenclature, "ADP-ribosyltransferase, diphtheria toxin-like" (ARTD), has been proposed in the field (Hottiger, 2015). Meanwhile, there are cellular enzymes that continuously remove ADP-ribosylation from modified proteins. Both poly(ADP-ribose) glycohydrase (PARG) and ADP-ribosylhydrolase 3 (ARH3) can facilitate the cleavage of ribose–ribose bonds within PAR polymers. Active isoforms of PARG can be found in both the cytoplasm and the nucleus while active ARH3 is mainly located in the cytoplasm, mitochondria and the nucleus (Slade et al., 2011; Niere et al., 2012; Mashimo, 2014). Other enzymes, such as ADP-ribosylarginine hydrolase 1 (ARH1) and MacroD2, can reverse MARylation processes. Although little is known about the biological role of mono-ADP-ribosylhydrolases, ARH1 specifically removes mono-ADP-ribose from the arginine residues of target proteins, whereas MacroD2 extends its activity to acidic residues, such as glutamate (Mashimo, 2014; Rosenthal et al., 2013).

The rapid addition and removal of ADPr units onto a variety of substrates allows cells to quickly adapt to different biological environments. Indeed, the significance of PARylation in regulating cellular processes that are critical for cell survival has been demonstrated. PARP1, the founding member of the PARP family, has been largely characterized for its involvement in DNA damage responses and chromatin remodeling. PARP1 can directly sense single-strand breaks upon DNA damage. Binding to DNA through its zinc finger domains, PARP1 relocates itself to the lesion sites and PARylates selected proteins involved in DNA repair (Langelier and Pascal, 2013). Additionally,

PARP1 can PARylate itself. Auto-PARylation is believed to prevent excessive binding and activity of PARP1 by charge–charge repulsion between the DNA phosphate backbone and PAR polymers (Zahradka and Ebisuzaki, 1982). At the same time, the modification is reversed by PARG to block hyper-PARylation. The dynamic process of PARylation with PARP1 and PARG leads to several consequences. First, branched PAR polymers at lesion sites serve as a scaffold to recruit downstream molecules, such as XRCC, through non-covalent interactions to initiate the DNA repair processes. Second, the branched PAR polymers result in the further amplification of stress signals to the close proximity of the lesion sites (Caldecott, 2003). Moreover, PARylation by PARP1 also facilitates chromatin remodeling during DNA damage response. Although the exact functions involved are still debatable, the remodeling event is believed to open up chromatin structures for repair and regulate the expression of certain transcription factors (Messner and Hottiger, 2011). Recent studies have also indicated the presence of PARylation in DNA double-strand break repair. Data suggest that multiple protein complexes, including BRCA1-BARD1 and RAP80, are recruited to the lesion sites by PARP1 activity at different time points during the repair processes (Li and Yu, 2013; Hu et al., 2014).

The discovery of PARP1 biological functions in DNA repair has led to the development of new therapeutics. PARP inhibitors, standalone or in combination with chemotherapy, have become a novel strategy to treat breast and ovarian cancers (Plummer, 2015). By inhibiting PARP1 activity and causing apoptosis in BRCA-deficient tumor cells, PARP inhibitors block single-strand break repair (Ashworth, 2008). On December 19th, 2014, a PARP1 inhibitor, Olaparib, was approved by the Food and Drug

Administration for clinical application in treating ovarian cancer patients (Olaparib Approved for Advanced Ovarian Cancer, 2015). Moreover, another PARP inhibitor rucaparib was granted breakthrough therapy designation by the FDA for treating ovarian cancer patients with *BRCA1/2* mutations (Kristeleit et al., 2015). Several other PARP inhibitors, including veliparib, niraparib, and talazoparib, are currently going through late phase clinical trials (Brown et al., 2016).

Beyond DNA repair, PARylation is also involved in other cellular regulations. For instance, poly(ADP-ribose)-dependent ubiquitination (PARdU), a novel pathway for protein degradation, has recently been discovered. Proteins modified by Tankyrase 1 and 2 (TNKS 1 & 2, also known as PARP 5a & 5b) are recognized by the E3 ubiquitin ligase RNF146 through its PAR-binding WWE domain, leading to proteasomal degradation (Zhang et al, 2011) (See also next two sections). Demonstrating a new level of complexity for cellular signaling pathways, PARdU serves as a cross-talk between PARylation and ubiquitination. Additionally, the role of PARylation in stress-granule formation has also been demonstrated. Five PARPs, namely, PARP 5a, 12, 13, 14, and 15, and two PARG isoforms haven been found to localize to stress granules (Leung et al., 2011). Overexpression of these PARPs results in stress granule formation without additional treatment. On the other hand, overexpression of PARGs prevents the assembly of stress granules. Furthermore, when PARG knockdown is performed, a prolonged presence of stress granules is observed after cellular stresses are removed. All these data suggest that PAR polymers provide a structural basis for the assembly of stress granules, and PARPs might be the driving force during this process (Leung et al., 2011, 2012). In addition, PARylation has been identified for its involvement in a variety of other cellular

processes, such as mitotic spindle assembly and telomere maintenance by PARP 5a (Chang et al., 2005; Ramamootthy and Smith, 2015).

Ubiquitination and E3 ligases

Ubiquitination is a post-translational modification that regulates protein stability, interaction, and localization in cells (Ye and Rape, 2009). The cellular ubiquitin system consists of several components: ubiquitin itself and E1, E2, and E3 enzymes. E1 enzymes, also known as ubiquitin-activation enzymes, uses ATP to activate free ubiquitin, which results in a conjugation formed by a thioester linkage between the active-site cysteine residue of E1 enzymes and the C-terminus of ubiquitin. Then, ubiquitin is transferred from the E1 to E2 and eventually passed along to the E3 (ubiquitin E3 ligase). Studies reveal that only a few E1 enzymes but over 600 E3s are present in mammalian cells (Welchman et al., 2005). As a result, the specificity of ubiquitination is mainly achieved through E3s. Ubiquitin can be linked through one of seven lysine residues or the N-terminus of the protein, which results in polyubiquitin with different linkages. The types of linkages within polyubiquitin chains specify the cellular functions of the modification. For instance, polyubiquitin chains with Lys48 linkage facilitates protein degradation through the proteasome; Chains with Lys63 linkage are associated with DNA repair, intracellular trafficking, protein–protein interactions, and ribosomal biogenesis (Li and Ye, 2008). E3 ligases can be categorized into two types on the basis of their ubiquitination activities. They either serve as catalytic enzymes, or they function as a platform to bring E2 and substrates in close proximity. Homologous to E6-AP Carboxy Terminus (HECT) E3 ligases use the former mechanism, whereas the latter

one is a feature shared by Really Interesting New Gene (RING) E3 ligases (Fang and Weissman, 2004). HECT-type E3s transfer ubiquitin from E2 to themselves and then continue the transfer to substrates.

RNF146

The RING-type ubiquitin E3 ligase RNF146 (also known as Iduna) was first discovered for regulating axin degradation in Wnt/β-catenin signaling pathway through a cross-talk between ubiquitination and PARylation (Zhang et al., 2011; Callow et al., 2011). PARylated axin is recognized by RNF146 and targeted for proteasomal degradation. Since β-catenin, a cell survival factor, is regulated by an axin-containing degradation complex, overexpression of RNF146 causes elevated levels of β-catenin and thus leads to enhanced tumor proliferation (Guo et al., 2013). Along with PARylated axin, auto-PARylated TNKS 1 & 2 have also been reported as substrates of RNF146 E3 ligase activity (Callow et al., 2011; Zhang et al., 2011). On the other hand, RNF146 has also been shown to have neuroprotective functions. Activation of NMDA receptors in glutamatergic neurons leads to upregulation of RNF146 expression. The ubiquitin E3 ligase is believed to counteract PARP1-promoted apoptosis after NMDA-induced excitotoxicity in a PAR-dependent manner (Andrabi et al., 2011). A later study also suggested that RNF146 can bind to PARylated DNA repair proteins, such as XRCC1, histones, Ku70, DNA ligase III, and PARP1 itself, to assist DNA damage repair in cells (Kang et al., 2011).

Understanding toward the complicated physiological roles of RNF146, as being either oncogenic or neural protective, cannot be achieved without further insights into the

molecular basis behind its ubiquitin E3 ligase activity. Despite the many studies reporting on the cellular functions of RNF146, only a few have examined the molecular mechanisms behind its effects. RNF146 consists of several domains/motifs. The RING domain sits near the amino-terminus of the RNF146 sequence, which is responsible for its ubiquitin E3 ligase activity, followed by a short linker region and then a domain called the WWE domain (see more in next section). The linker region provides the flexibility for two domains to carry out their functions properly. The WWE domain has been identified for its binding affinity for *iso*-ADP ribose (*iso*-ADPr), an internal unit of the PAR polymer (Figure 1, adapted from Leung, 2014). The long and unstructured region at the carboxyl-terminus of RNF146 presumably contains several motifs for interactions with TNKS (DaRosa et al., 2015). Using GST-tagged wild-type RNF146 was able to pull down the TNKS five ankyrin repeat clusters (TNKS 5ARC) fragment in vitro while mutants with a truncated or mutated C-terminus failed to do so (DaRosa et al., 2015). Nonetheless, the exact mechanism behind the interaction between TNKS and RNF146 is still unclear. As a RING-type E3 ligase, RNF146 can directly transfer ubiquitin from E2 ligases to substrates. In addition, ubiquitination by RNF146 is robustly increased from the basal level when it binds to PARylated substrates through its WWE domain. Tracing the rate of ubiquitin transfer from the E2-ubiquitin complex to a free lysine *in vitro* can qualitatively measure and compare the E3 ligase activity of RNF146 with or without binding to PAR. Addition of purified *iso*-ADPr or PAR polymers, but not ADPr, to full-length RNF146 could completely release ubiquitin from the UbcH5c(E2)-ubiquitin complex to a free lysine within 4 minutes. In contrary, without addition of *iso*-ADPr or PAR, the majority of ubiquitin remain bound to the E2-ubiquitin complex within the 4-

minute time period (DaRosa et al., 2015). Moreover, measuring the rate of ubiquitn transfer using the RING–WWE fragment of RNF146 gives a comparable result, indicating that the RING–WWE region is the basic functioning unit of RNF146 for its E3 ligase activity.

The partial crystal structure indicates the binding of *iso*-ADPr between the RING and WWE domains through its contact with several residues in both domains. On the other hand, phosphate groups on both sides of *iso*-ADPr are exposed to the outside, which explains how RNF146 can interact with PAR polymers (Wang et al., 2011). Additionally, the binding to *iso*-ADPr triggers a conformational change in the RING domain that favors E2 interaction. The stabilization of the E2–E3 interface translates into elevated ubiquitination activity by RNF146. An additional mutagenesis study revealed the details behind such a phenomenon. Lys 61 couples ligand binding to the activation of the RING domain by facilitating the formation of a central helix that orients the two Zn^{2+} loops for E2 binding. On the other hand, Gly 62 and Trp 65 help stabilize the inactive form by disrupting helix formation. The substitution of Lys 61 to Ala or Asp abolishes the activation of E3 ligase activity while the mutant can still bind to *iso*-ADPr. On the contrary, mutations in Gly 62 and Trp 65 increase the basal level of E3 activity (DaRosa et al., 2015). A second study confirms that mutations in similar regions of RNF146 affect its E3 ligase activity (Kang et al., 2011). In summary, the current experimental evidence supports a model in which binding of PAR chains derived from PARylated proteins activates RNF146 ubiquitin E3 ligase activity by triggering a conformational change in the inactive RING domain, which leads to ubiquitination and protein degradation by the proteasome.

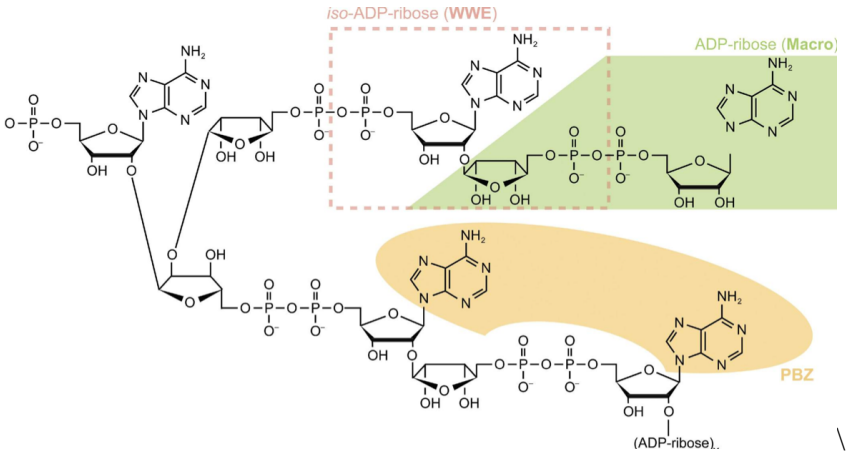

Figure 1 | Structure of poly(ADP-ribose) polymers and its interacting domains. The minimum structural units within PAR that are recognized by each interacting domains are highlighted. The WWE domain is capable of binding to iso-ADP-ribose motifs; Marco domains recognize distal ADP-ribose motifs while PBZ domains interact with two adenosine groups of ADP-ribose motifs (adapted from Leung, Anthony K.L., 2015)

WWE domains

WWE domains were first identified by a multiple sequence alignment using PSI-BLAST (Aravind, 2001). The domain was named after the three conserved residues within the sequences, Trp(W), Trp (W), and Glu (E). A secondary-structure prediction as well as NMR structures indicated the presence of multiple beta-strands and a central alpha-helix, as common features shared by members of the WWE family (He et al.,

2012). The best-described member is the RNF146 WWE domain. The crystal structure, along with the mutagenesis study, has demonstrated the molecular basis for binding *iso*-ADPr by the RNF146 domain. The RNF146 WWE domain forms a half beta barrel structure that consists of six beta sheets and a central alpha-helix between the second and third sheets. The surface of the binding pocket within the half beta barrel is positively charged, which allows the accommodation of *iso*-ADPr. Within the pocket, Tyr144 and Arg163 make contact with the phosphate group on one side of *iso*-ADPr, whereas Arg110, Trp114, and Lys175 interact with the other phosphate group and ribose (Figure 2a, adapted from Wang et al., 2012). The unique interaction between residues and two phosphate groups on both sides provided the rationale for the specificity of the RNF146 WWE domain toward *iso*-ADPr but not ADPr. On the other hand, the fact that both ends of *iso*-ADPr are exposed when it is bound by the WWE domain further provides evidence of how RNF146 can bind to PAR polymers. Moreover, the hydrogen bonding formed by Gln153 with the adenine ring, as well as the stacking effect by the Tyr107 phenol group, also assists the positioning of the adenine ring and the ribose group in the binding pocket of the RNF146 WWE domain. Data generated by isothermal titration calorimetry (ITC) have shown that changing Tyr107, Tyr144A, or Arg163 to Ala will abolish the *iso*-ADPr binding affinity of the RNF146 WWE domain (Figure 2b, adapted from Wang et al., 2012).

a

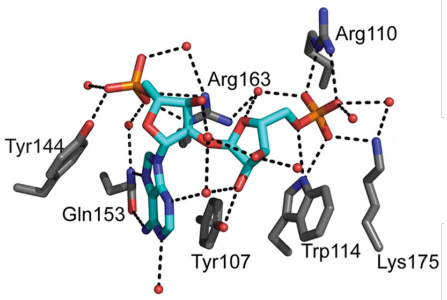

b

RNF146 WWE domain	Kd measured by ITC for *iso*-ADPR(μM)
Wild type	0.37 ± 0.02
Y107A	No binding
R110A	1.01 ± 0.05
W114A	32.79 ± 0.15
Y144A	No binding
Q153A	10.71 ± 0.12
R163A	No binding
K175A	1.22 ± 0.18

Figure 2 | Recognition of iso-ADPr motif by RNF146 WWE domain. a) Key residues in RNF146 WWE domain that are involved in binding iso-ADPr. Hydrogen bonds are represented by dashed lines. Water molecules are represented by red spheres. b) Mutagenesis analysis of key residues in RNF146 WWE domain for *iso*-ADPr binding. Dissociation constants shown in the table were measured by isothermal titration calorimetry (ITC) analysis (adapted from Wang et al., 2012).

Although the RNF146 WWE domain has been largely studied, little is known about other WWE domains, especially those that are found in proteins within mammalian cells. Recognition of *iso*-ADPr is likely a common feature of WWE domains, with a few exceptions. In particular, a functional resemblance in PAR interaction among E3 ligase WWE domains exists (Wang et al., 2011). By contrast, the true nature of PARP WWE domains, and most importantly, how these domains contribute to PARP activities, remain unclear. To date, 12 mammalian proteins have been identified to carry WWE domain(s) (Figure 3, adapted from Kalisch et al., 2012). Among them, RNF146, HUWE1, TRIP12, and Deltex 1, 2, and 4 are ubiquitin E3 ligases, whereas tiPARP (PARP7) and PARP 11, 12, 13, and 14 are PAR polymerases. DDHD2 is the only phospholipase found with a

WWE domain within the structure. Deltex 1, 2, and 4, as well as PARP 12, contain two WWE domains, and the rest contain only one (Kalisch et al., 2012).

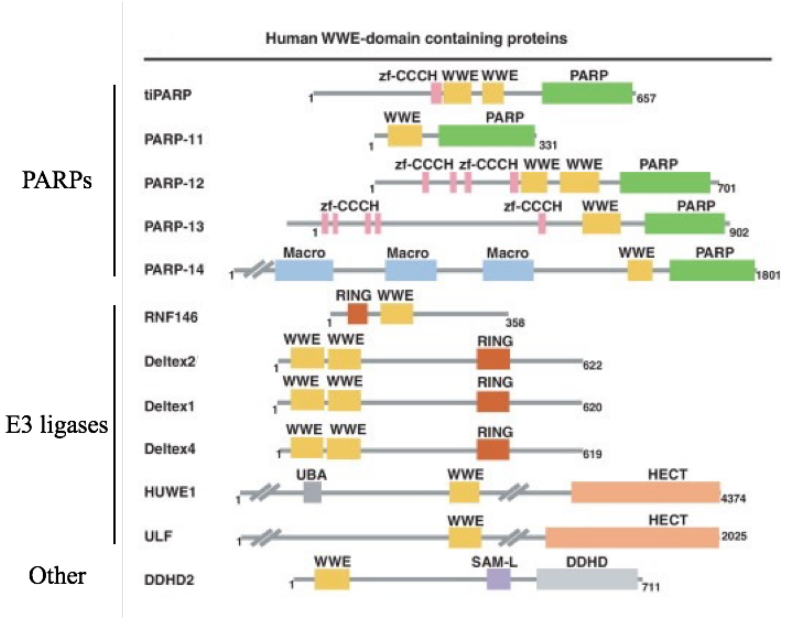

Figure 3 | Schematic diagram for human WWE-domain containing proteins. WWE domains in each protein are highlighted in yellow (adapted from Kalisch et al., 2012).

PAR induction – a novel phenomenon of RNF146 and its WWE domain

As a master mediator between ubiquitination and PARylation pathways, RNF146 has caught our attention. Intriguingly, our curiosity toward RNF146 and other WWE domain-containing proteins has led us to discover a new property of RNF146 from an experimental control. Previous work, done by my lab colleague Dr. Yoshinari Ando (unpublished data), suggested that overexpression of mouse RNF146 or its WWE domain in 293F cells, but not PARP13.1, 13.2, or GFP alone, were able to increase signals for endogenous PAR in cell lysates detected by western blot (Figure 4). Given that all samples went through the same preparation, the elevated cellular PAR level was unlikely

due to the transfection procedure. Additionally, even though GFP was expressed at a higher level, it failed to induce the cellular level of PAR. Thus, it is also unlikely that the increased PAR signal was due to the amount of protein overexpression. Although the WWE domain was a common feature shared by PARP13.1, PARP13.2, and mouse RNF146 (mRNF146), only overexpression of RNF146 increased cellular PAR levels detected on western blot, suggesting that this property is not shared by overexpression of any WWE domain-containing protein. Here, in this thesis, we further characterize RNF146 and the role of its WWE domain in affecting PAR levels in the cell, as well as explore the possibility of engineering the RNF146 WWE domain into a molecular tool for modulating cellular PARylation events.

(Next Page) Figure 4 | Overexpression of mouse RNF146 (mRNF146) and its WWE domain result in elevated levels of cellular PAR. Western blots of total cell lysates from 293F cells expressing GFP, GFP-tagged PARP13.1, PARP13.2, mRNF146 and mRNF146 WWE domain using antibodies against PAR (left) and GFP (right). (Data contributed by Dr. Yoshinari Ando)

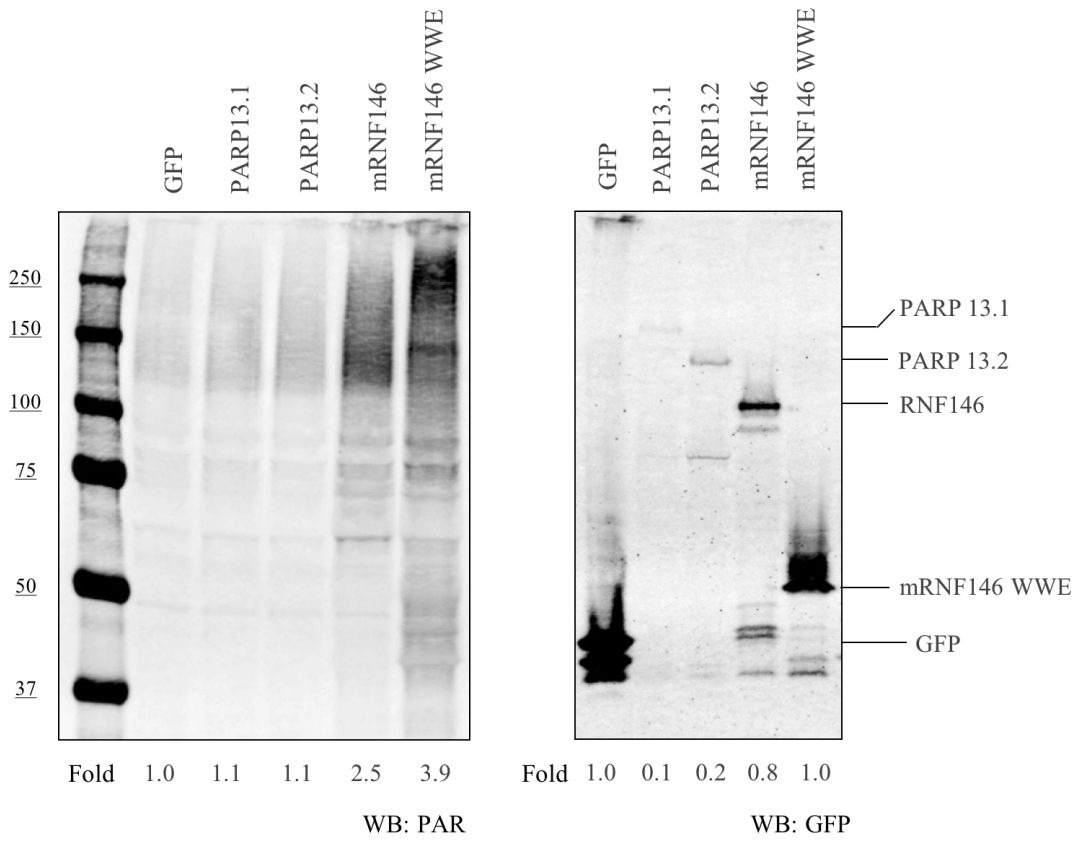
GFP
PARP13.1
PARP13.2
mRNF146
mRNF146 WWE
250
150
100
75
50
37
Fold 1.0 1.1 1.1 2.5 3.9
WB: PAR
GFP
PARP13.1
PARP13.2
mRNF146
mRNF146 WWE
PARP 13.1
PARP 13.2
RNF146
mRNF146 WWE
GFP
Fold 1.0 0.1 0.2 0.8 1.0
WB: GFP

Material and Methods

HEK293F cell transfection and harvesting

Twenty milliliters of HEK293F cells were seeded at 5 x 10^5 cells/mL density in a 125 mL flask the day before transfection. The cells were incubated at 37 °C with 8% CO_2 content and then shaken constantly at a speed of 135 rpm for 24 h.

Plasmid DNA was added to a 230 µL solution of Opti-MEM (31985070, Gibco) as mixture A. Then, 20 µL of 293fectin (12347-019, Invitrogen) was mixed with 230 µL of Opti-MEM and incubated at room temperature for 5 min as mixture B. Mixtures A and B were combined and incubated for 20 min at room temperature. The solution was then added to the cell culture before the transfected cells were incubated for another 24 h at 37 °C with 8% CO_2 content and shaken constantly at a speed of 135 rpm.

The transfected HEK293F cells were collected after being spun down at 400 xg for 5 min. The cell pellets were washed with 10 mL of cold PBS (10010-049, Gibco). The cell pellets were then lysed on ice for 10 min with the use of mRIPA buffer (50 mM Tris-HCl pH7.4, 150 mM NaCl, 0.1% sodium deoxycholate, 1% NP-40, 1 mM EDTA pH 8.0, 1x SigmaFast Protease Inhibitor) with 1 µM ADP-HPD (118415, EMD Millipore). The supernatant was collected after a spin-down solution at 14,000 rpm for 15 min at 4 °C. Then, 0.25 µL of 1 mg/mL cytochalasin (sc-201442, Santa Cruz) was added to the cell lysates and incubated on ice for 10 min. The lysates were diluted with 2x protein loading buffer (62.5 mM Tis-HCL pH6.8, 25% glycerol, 2%SDS, and 0.1% Orange G dye) before Western blot analysis.

HEK293T cell transfection and harvesting

Two milliliters of HEK293T cells were seeded at 5 x 10^5 cells/mL density in a six-well plate (82050-842, Cellstar) the day before transfection. The cells were incubated in a cell chamber at 37 °C and 5% CO_2 content for 24 h.

Before transfection, the amount of cell medium was reduced to 1 mL per well. Plasmid DNA was added to 150 μL solution of Opti-MEM as mixture A. Six microliters of Lipofectamine™ 2000 (1168027, invitrogen) was mixed with 230 μL of Opti-MEM and incubated at room temperature for 5 min as mixture B. Mixtures A and B were then combined and incubated for 10 min at room temperature. The solution was added to the cell medium in each well. The transfected cells were incubated for another 24 h at 37 °C with 5% CO_2 content.

The six-well plate was placed on ice before harvesting. The transfected cells were collected with 1.5 mL of cold PBS and spun down at 400 xg for 5 min after removal of the medium. The cell pellets were lysed with 150 μL 1x protein loading (31.25 mM Tis-HCL pH 6.8, 12.5% glycerol, 1% SDS, and 0.05% Orange G dye). The cell lysates were transferred to QIAshedder tubes (79656, Qiagen) and spun down at 14,000 rpm for 2 min to remove high-molecule-weight genomic DNA and other viscous cell components.

HeLa cell/DLD1 cell transfection and harvesting

The cell seeding and transfection processes were the same, as indicated in the *HEK293T cell transfection and harvesting* section, except for a change of the cell medium used for the HeLa cells at a 6 hr time point after transfection.

The six-well plate was placed on ice before harvesting. The transfected cells were washed twice with 1 mL of cold PBS after removal of the medium. Then, 150 µL 1x protein loading buffer was used to lyse the cells in each well. The cell lysates were transferred to QIAshedder tubes and spun down at 14,000 rpm for 2 min to remove high-molecule-weight genomic DNA and other viscous cell components.

Western Blot

The cell lysates were heated at 95 °C for 5 min before they were loaded on a home-made 10% SDS-PAGE gel (30% polyacrylamide, 25% 1.5 M Tris-HCL pH 8.8, 10% ammonium persulfate, 10% SDS 1% TEMED). The samples were run at 150 V until the loading dye passed the bottom of the gel; they were then transferred onto a nitrocellulose membrane (GE10600007, Sigma-Aldrich) with either overnight wet transfer (at 12 V for 16 h) or semi-dry transfer (at 15 V for 50 min) method. The membrane was blocked with 4% skin milk (A614-1000, Quality Biological) in TBS (20 mM Tris-HCl pH 7.4, 150 mM NaCl) for 1 h at room temperature. The primary antibody was diluted in TBST (20 mM Tris-HCl pH 7.4, 150 mM NaCl, 0.1% Tween20, 0.01% thimerosa) and incubated with membrane at 4 °C overnight. After three 10-minute washes with TBST, the membrane was incubated with a secondary antibody (diluted in 15 mL of 4% skin milk in TBST) for 40 min. The membrane was scanned on a LI-COR Odyssey Imager after three additional 10-minute washes with TBST. The following antibodies were used for Western blot: rabbit polyclonal anti-PAR antibody (4336-BPC, Trivegen, USA), mouse anti-GFP (11814460001, Roche, USA), rabbit anti-TNKS 1&2

(H-350) (sc-8337, Santa Cruz, USA), anti-axin (AF3287, R&D System, USA), and mouse anti-PAN-ADPr (MABE1016, Millipore, USA).

PCR protocol

For the PCR reaction using Q5 polymerase (M0491L, NEB), the reaction mixture was set up as follows:

5X Q5 Reaction buffer – 5 µl

10 mM dNTPs – 0.5 µl

10 µM Forward Primer – 1.25 µl

10 µM Reverse Primer – 1.25 µl

Template Plasmic DNA – 4 µl

Q5 polymerase – 0.25 µl

5X Q5 Enhancer – 5 µl

ddH2O

Total: 25 µL

The Q5 PCR reaction steps were as follows:

1. 98 °C, 1 min

2. 98 °C, 20 sec

3. Lowest Tm + 3 °C, 30 sec

4. 72 °C, 30 sec/kb

5. 72 °C, 2 min

6. 4 °C, ∞

*Repeat steps 2–4 30 times

For the PCR reaction using Taq polymerase (M0267L, NEB), the reaction mixture was set up as follows:

10x Thermo buffer – 2.5 µL

10 µM FP.for primer – 0.5 µL

10 µM FP.rev primer – 0.5 µL

dNTP mix – 0.5 µL

colony DNA as template

ddH2O –18.875 µL

NEB Taq polymerase – 0.125 µL

Total: 25 µL

The Q5 PCR reaction steps were as follows:

1. 95 °C, 3 min

2. 95 °C, 20 sec

3. Tm: 5 °C, 30 sec

4. 68 °C, 30 sec/kb

5. 68 °C, 5 min

6. 4 °C, ∞

*Repeat steps 2–4 30x

Restriction enzyme digestion

The reactions for double-enzyme digestion were carried out with FastDigest restriction enzymes (XhoI-FD0694, BamHI-FD0054, HindIII-FD0504, BbsI-FD1014, EcoRI-FD0274, PstI-FD0614, Thermo Fisher) and FastAP alkaline phosphatase (EF0651, Thermo Fisher).

The reaction mixture for processing the vector plasmid was set up as follows:

Plasmid DNA – 3 μg

10 x FastDigest Buffer – 2 μL

FastDigest enzyme I – 1 μL

FastDigest enzyme II – 1 μL

FastAP alkaline phosphatase – 1μL

ddH2O

Total: 20 μL

The reaction was mixed thoroughly with constant shaking and then incubated at 37 °C for 30 min. The reaction products were analyzed on 1% agarose gel. The DNA fragments with correct size were purified with a Qiagen Gel purification kit (28704, Qiagen). The manufacturer's protocol was followed for the PCR purification.

The reaction mixture for processing the DNA insert was set up as follows:

DNA insert – 10 µL

10 x FastDigest Buffer – 2 µL

FastDigest enzyme I – 1 µL

FastDigest enzyme II – 1 µL

ddH2O

Total: 20 µL

The reaction was mixed thoroughly with constant shaking and then incubated at 37 °C for 30 min. The reaction products were purified with Qiagen PCR purification kit (28104, Qiagen). The manufacturer's protocol was followed for PCR purification.

Bacterial transformation

SoloPack® Gold supercompetent cells (230350, Agilent Technologies) were used for bacterial transformation. One microliter of ligation reaction product was added to10 µL of the competent cells for each transformation reaction. After a 30 min incubation on ice, the competent cells were heat-shocked at 42 °C for 30 s and then incubated on ice for an additional 2 min. A 30 min recovery at 37 °C with a 300 µL pre-warmed SOC

medium (340-031-671, Quality Biological) was performed before the cells were spread onto an LB/agar plate with antibiotics for colony selection.

Colony screening was performed with Taq polymerase PCR reaction, as described above, to check the correct insertion of DNA sequences into the vector. Miniprep kit (A1222, Promega) and maxiprep kit (11-555(D4202), Genesee Scientific (Zymo research)) were used for plasmid extraction. The manufacturer's protocol was followed for the miniprep and maxiprep reactions. The plasmids were then sent for sequencing (Genewiz). Glycerol (G5516, Sigma-Aldrich) stock (400 µL glycerol + 600 µL bacterial culture) was made and stored in an −80 °C freezer for each bacterial strain carrying the correct plasmids.

Site-directed mutagenesis (SDM)

Partially overlapping primers were designed to improve the efficiency of PCR reaction. A PCR reaction (with SDM primers) using Q5 polymerase was carried out, as described above. The PCR products were digested with 1 µL DPNI (R0176L, NEB) at 37 °C for 1 h to remove template DNA. The digestion product was then transformed into competent cells, as described above.

Immunofluorescence microscopy

Arsenite treatment

A mammalian cell culture was prepared, as described above. Two hundred and fifty microliters 1 mg/mL sodium arsenite (35000, Fluka) was added to a 2250 µL cell medium to reach a final concentration of 100 µg/mL. The cells were then incubated at

37 °C and 5% CO_2 content for 30 min. A wash with cold PBS was performed to remove sodium arsenite before cell harvesting.

Hydrogen peroxide treatment

A mammalian cell culture was prepared, as described above; 0.4 µL 30% (w/w) hydrogen peroxide (311448, Sigma) was diluted with a 250 µL medium. The mixture was then added to a 2 mL cell medium in each well to reach a final concentration of 1 µM per well. The cells were then incubated at 37 °C and 5% CO_2 content for 10 min. A wash with cold PBS was performed to remove hydrogen peroxide before cell harvesting.

PFA fixation

Sterilized cover glasses were placed in each well of the six-well plate before cell seeding. A wash with PBS was performed to remove residual ethanol from the sterilization process. HeLa cells were seeded, incubated, and transfected, as described previously. After a 24 h incubation, the cover glasses were transferred to a 24-well plate and washed with PBS. Then, 4% PFA (15714, Electron Microscopy Science) in PBS was added in each well for cell fixation. After a 10 min incubation, the cover glasses were washed with PBS to remove PFA. The cover glasses were then incubated with 1% Triton X-100 (T8787, Sigma) in PBS at room temperature for 10 min to permeabilize the cell membrane, followed by an additional wash with PBS. The cells were then blocked with 1% donkey serum in PBST (137 mM NaCl, 2.7 mM KCl, 10 mM Na_2HPO_4, 1.8 mM KH_2PO_4) at room temperature for 30 min. Primary antibody (1:100 in PBST with 1% donkey serum) was added on top of each cover glass and incubated at room temperature

for 1 h. The cover glasses were then washed with PBST three times before they were incubated with the diluted secondary antibody (1:500 in PBST with 1% donkey serum) for 30 min, followed by an additional wash with PBST. The cover glasses were stained with 1 μM DAPI for 5 min and rinsed with PBS before they were fixed on slides with ProLong Gold® Antifade Mountant (P36934, Life Technologies). A layer of nail polisher was applied around the cover glasses to seal the gap. The slides were visualized with a DeltaVision Elite deconvolution microscope (29065728, GE healthcare Life Science). The following antibodies were used for immunofluorescence microscopy: rabbit polyclonal anti-PAR antibody (4336-BPC, Trevigen, USA), mouse anti-GFP (11814460001, Roche, USA), rabbit anti-TNKS 1&2 (H-350) (sc-8337, Santa Cruz, USA), anti-axin (AF3287, R&D System, USA), and goat anti-eIF3η (sc-16377, Santa Cruz Biotechnology, USA).

Methanol fixation

The steps were the same as described in the PFA fixation, except for the use of methanol for cell fixing and permeabilization instead of 4% PFA and 1% Triton X-100. One milliliter of cold methanol (100208, Thermo Fisher) was added to each well and incubated for 5 min at room temperature, followed by slow rehydration with PBS.

Table I. List of PCR Primers

Primer	Sequence	Note
HW001_RNF146_sgRNA-1_plus	CAC CGT CTT TAA CCG TCC CTG AAT G	sgRNA-plus-RNF146-CRSIPR-MIT-01
HW002_RNF146_sgRNA-1_minus	AAA CCA TTC AGG GAC GGT TAA AGA C	sgRNA-minus-RNF146-CRSIPR-MIT-01
HW003_RNF146_sgRNA-2_plus	CAC CGA CAA ACA GGA AAG CGA ACG A	sgRNA-plus-RNF146-CRSIPR-MIT-02
HW004_RNF146_sgRNA-2_minus	AAA CTC GTT CGC TTT CCT GTT TGT C	sgRNA-minus-RNF146-CRSIPR-MIT-02
HW005_RNF146_sgRNA-3_plus	CAC CGT AAG CAC GTT TTC TGC TAT	sgRNA-plus-RNF146-Benchling-01
HW006_RNF146_sgRNA-3_minus	AAA CAT AGC AGA AAA CGT GCT TAC	sgRNA-minus-RNF146-Benchling-01
HW007_PARP5a_sgRNA-1_plus	CAC CGC AGT CGG GAT CCG CCC GAC	sgRNA-plus-PARP5a-CRSIPR-MIT-01
HW008_PARP5a_sgRNA-1_minus	AAA CGT CGG GCG GAT CCC GAC TGC	sgRNA-minus-PARP5a-CRSIPR-MIT-01
HW009_PARP5a_sgRNA-2_plus	CAC CGA CAG CTC CAG CCC GCC CCA G	sgRNA-plus-PARP5a-ECRSIPR-01
HW010_PARP5a_sgRNA-2_minus	AAA CCT GGG GCG GGC TGG AGC TGT C	sgRNA-minus-PARP5a-ECRSIPR-01
HW011_PARP5a_sgRNA-3_plus	CAC CGC ACG GCC TAG CGC TGC CGG	sgRNA-plus-PARP5a-CHOPCHOP-01
HW012_PARP5a_sgRNA-3_minus	AAA CCC GGC AGC GCT AGG CCG TGC	sgRNA-minus-PARP5a-CHOPCHOP-01
HW013_PARP5b_sgRNA-1_plus	CAC CGC TGT TCG AGG CGT GCC GCA A	sgRNA-plus-PARP5b-CRSIPR-MIT-01
HW014_PARP5b_sgRNA-1_minus	AAA CTT GCG GCA CGC CTC GAA CAG C	sgRNA-minus-PARP5b-CRSIPR-MIT-01
HW015_PARP5b_sgRNA-2_plus	CAC CGG CCG CCC GAG AGC TGT TCG	sgRNA-plus-PARP5b-ECRSIPR-01
HW016_PARP5b_sgRNA-2_minus	AAA CCG AAC AGC TCT CGG GCG GCC	sgRNA-minus-PARP5b-ECRSIPR-01
HW017_PARP5b_sgRNA-3_plus	CAC CGA TGT CGG GTC GCC GCT GCG C	sgRNA-plus-PARP5b-Benchling-01
HW018_PARP5b_sgRNA-3_minus	AAA CGC GCA GCG GCG ACC CGA CAT C	sgRNA-minus-PARP5b-Benchling-01
HW019_pSpCas9_F (4-23)	GGCCTATTTCCCATGATTCC	Universal DNA primers for amplification of target insertion region (327 bp) on pSpCas9 (BB)-2A-GFP (px458) plasmid
HW020_pSpCas9_R (308-330)	GCCACTTTTTCAAGTTGATAA CG	Universal DNA primers for amplification of target insertion region (327 bp) on pSpCas9 (BB)-2A-GFP (px458) plasmid
HW021_SURVEYOR_RNF146_F	CCT TTT CCC CTC ACT GGA TGC	Primers for SURYEYOR assay
HW022_SURVEYOR_RNF146_R	GCT TGT CAA GGA AAT CCT CGG G	Primers for SURYEYOR assay
HW023_SURVEYOR_TNKS1_F	CCG TTC CCT TGG CTG TTC TCT	Primers for SURYEYOR assay
HW024_SURVEYOR_TNKS1_R	CGG GGA AGA AGA GGA CGA CG	Primers for SURYEYOR assay

Primer	Sequence	Note
HW025_SURVEYOR_TNKS2_F	GAT CCG GTG ACA GCA GGG AG	Primers for SURYEYOR assay
HW026_SURVEYOR_TNKS2_R	GTC CCC ACT GGA AGA GAG CG	Primers for SURYEYOR assay
HW027_hRNF146_Forward	GTC TCG AGC TAT GGC TGG CTG TGG TGA AAT TG	Primer for cloning human RNF146
HW028_hRNF146_Reverse	GTG GAT CCT TAA ACT TCA GTT ACT GTG	Primer for cloning human RNF147
HW029_hRNF146_Q153A_Forward	TCG CTG ATC TTG AAA ACA TGG TTG CAT ATA GGA GAA ATG AAC ATG GAC	Primer for SDM human RNF146
HW030_hRNF146_Q153A_Reverse	GTC CAT GTT CAT TTC TCC TAT ATG CAA CCA TGT TTT CAA GAT CAG CGA	Primer for SDM human RNF147
HW031_5GEX_hRNF146_C-tar	GGG CTG GCA AGC CAC GTT TGG TG	Sequencing primer
HW032_3GEX_hRNF146_C-tar	CCG GGA GCT GCA TGT GTC AGA GG	Sequencing primer
HW033_T7tem_hRNF146_FL	GCT AGT TAT TGC TCA GCG G	Sequencing primer
HW034_T7prom_hRNF146_FL	TAA TAC GAC TCA CTA TAG GGG AAT TG	Sequencing primer
HW033_hRNF146_RING_WWE_Forward	GTC TCG AGC TCC TTC TTT AAC CGT CCC TGA ATG TG	Primer for cloning human RNF146 RING-WWE
HW034_hRNF146_RING_WWE_Reverse	GTG GAT CCT TAT AGC CTA AGT CCA GCT ACT CCC TTC	Primer for cloning human RNF146 RING-WWE
HW035_hRNF146_WWE_Ctar_Forward	GTC TCG AGC TAA TGG TGA ATA TGC ATG GTA TTA TGA AGG AAG	Primer for cloning human RNF146 WWE-Cter
HW036_hRNF146_WWE_Ctar_Reverse	GTG GAT CCT TAA ACT TCA GTT ACT GTG CAC TGT CCA TC	Primer for cloning human RNF146 WWE-Cter
HW039_PARP7 WWE cloning For	GCG TCT CGA GTA ATT TAC CAC ACA GTC TGG AAA TTC TTC	Primer for cloning human PARP 7 WWE
HW040_PARP7 WWE cloning Rev	GCT GGA TCC TTA CTG TAA ATA TGG AAG CAG TAT AAA ACA GG	Primer for cloning human PARP 7 WWE
HW041_PARP11 WWE cloning For	GCG TCT CGA GTA GAT ACC CAG TGG GGC TGG	Primer for cloning human PARP 11 WWE
HW042_PARP11 WWE cloning Rev	GCT GGA TCC TTA CTC GTT TTC ACA GAT GTA ACT GAA AGC	Primer for cloning human PARP 11 WWE
HW043_PARP13 WWE cloning For	GCG TCT CGA GTA ACC ACC AAA TGG ATT TGG TAT TGG	Primer for cloning human PARP 13 WWE
HW044_PARP13 WWE cloning Rev	GCT GGA TCC TTA TCT CTT CAT CTG CTG CAC ATA CC	Primer for cloning human PARP 13 WWE
HW045_PARP14 WWE cloning For	GCG TCT CGA GTA GAA CAG GAA TCC CGG GC	Primer for cloning human PARP 14 WWE
HW046_PARP14 WWE cloning Rev	GCT GGA TCC TTA CAT ATC ACT CCA GTG TGC AGG	Primer for cloning human PARP 14 WWE
HW047_PARP12 WWE1 cloning For	GCG TCT CGA GTA CAT TTG CCG TAT CGA TGG CAA	Primer for cloning human PARP 12 WWE (1st)

Primer	Sequence	Note
HW048_PARP12 WWE1 cloning Rev	GCA TGA ATT CTT AGA GGA TGA AGT GTG GAG GTT TG	Primer for cloning human PARP 12 WWE (1st)
HW049_PARP12 WWE2 cloning For	GCG TCT CGA GTA ACC ACT GAC TGG ATT TGG TAC TG	Primer for cloning human PARP 12 WWE (2nd)
HW050_PARP12 WWE2 cloning Rev	GCA TGA ATT CTT AGG TTT GCA TGG TCG TCA CAT C	Primer for cloning human PARP 12 WWE (2nd)
HW051_mito-WWE(RNF146) Forward	GCT GGA TCC TAA TGG TGA ATA TGC ATG GTA TTA TGA AGG AAG	Primer for cloning Mitochondria-WWE(hRNF146)
HW052_mito-WWE(RNF146) Reverse	GCA ACC GGT GCT AGC CTA AGT CCA GCT ACT CCC TTC	Primer for cloning Mitochondria-WWE(hRNF146)
HW053_FPN1.rev	GTC GCC GTC CAG CTC GAC CAG	Sequencing primer
HW055_SDM_hRING_K61A_Forward	GCA CGT TTT CTG CTA TCT ATG TGT AGC AGG AGC TTC ATG GCT	Primer for SDM RING Domain (human RNF146)
HW056_SDM_hRING_K61A_Reverse	AGC CAT GAA GCT CCT GCT ACA CAT AGA TAG CAG AAA ACG TGC	Primer for SDM RING Domain (human RNF146)
HW057_RNF146 K61A non-overlapping rev.	CAT AGA TAG CAG AAA ACG TGC TTA CAG GGC AGA CTG ACT G	Primer for SDM RING Domain (human RNF146)
HW059_hULF-WWE for.	CGT ACG AAT TCA GGA AAT GCA CAG AAC ACA GAT GG	Primer for cloning human ULF WWE
HW060_ hULF-WWE rev.	GTG GAT CCC TAA AGC TGT GCT CGA GCA TC	Primer for cloning human ULF WWE
HW061_R163A SDM for.	GTC GCG CGA AGA TTA AGC GAG ATA TAA TAG ATA TAC CAA AGA AGG G	Primer for SDM WWE Domain (human RNF146)
HW062_R163A SDM rev.	CTT AAT CTT CGC GCG ACG TCC ATG TTC ATT TCT CCT ATA TTG AAC	Primer for SDM WWE Domain (human RNF146)
HW063_Y144A SDM for.	CTT TCT GGC TGT CGC TGA TCT TGA AAA CAT GGT TCA ATA TAG GAG	Primer for SDM WWE Domain (human RNF146)
HW064_Y144A SDM rev.	CAG CGA CAG CCA GAA AGC CAG CAA TTA ACA TTT CAG TGT TC	Primer for SDM WWE Domain (human RNF146)
HW065_mDDHD2 WWE for.	GTC TCG AGC TTC CTT CGA ACT CAT AGA CAT GGA C	Primer for cloning mouse DDHD2 WWE
HW066_mDDHD2 WWE rev.	GTG GAT CCT TAA GAC CCT GCA ATT GGC TG	Primer for cloning mouse DDHD2 WWE
HW067_mDeltex1 WWE for	GTC TCG AGC TAA CGT GGC CAG GGT GG	Primer for cloning mouse Deltex1 WWE
HW068_mDeltex1 WWE rev.	GTG GAT CCT TAT TGC GAC TTG GGA ATG GAG C	Primer for cloning mouse Deltex1 WWE
HW069_New 1st WWE For.	GCA TCT CGA GCT AAT GGT GAG TAC GCT TGG TAC TAC	Primer for PCR amplification of synthesized oligos of 1st WWE domain (XhoI-WWE-HindIII)
HW069_New 1st WWE Rev.	GCT CAA GCT TGA GTC TCA GAC CCG CAA CAC C	Primer for PCR amplification of synthesized oligos of 1st WWE domain (XhoI-WWE-HindIII)

Table II. List of cloned DNA constructs

Name
pEGPFP-hRNF146
pEGPFP-hRNF146 WWE
pEGPFP-hRNF146 RING-WWE
pEGPFP-hRNF146 WWE-Cter
pEGPFP-PARP7 WWE
pEGPFP-PARP11 WWE
pEGPFP-PARP12 WWE (1st)
pEGPFP-PARP12 WWE (2nd)
pEGPFP-PARP12 WWE-WWE
pEGPFP-mito-WWE
pEGFP-mDeltex 1WWE
pEGFP-hULF WWE
pEGFP-hRNF146 WWE Y144A
pEGFP-hRNF146 WWE R163A
pEGFP-linker-(2nd)WWE
pEGFP-linker-(2nd)WWE-NES
pEGFP-linker-(2nd)WWE-NLS
pEGFP-WWE-WWE
pEGFP-WWE-WWE-NLS
pEGFP-WWE-WWE-NES
pSpCas9 (anti-RNF146 sgRNA1) HW 001/002
pSpCas9 (anti-RNF146 sgRNA2) HW 003/004
pSpCas9 (anti-RNF146 sgRNA3) HW 005/006
pSpCas9 (anti-TNKS1 sgRNA1) HW 007/008
pSpCas9 (anti-TNKS1 sgRNA2) HW 009/010
pSpCas9 (anti-TNKS1 sgRNA3) HW 011/012
pSpCas9 (anti-TNKS2 sgRNA1) HW 013/014
pSpCas9 (anti-TNKS2 sgRNA2) HW 015/016
pSpCas9 (anti-TNKS2 sgRNA3) HW 017/018

Results

Overexpression of human RNF146 mimics the PAR-induction effect by mouse RNF146 to a lesser extent

Amino acid sequence alignments showed that mouse and human RNF146 (mRNF146 and hRNF146) share 92% overall homology (Figure 5a). Moreover, the RING and WWE domains are 100% identical. We therefore investigated whether expression of hRNF146 could lead to a similar induction of endogenous PAR levels observed in cells expressing mRNF146. The cDNA of hRNF146 was cloned into the GFP expression vector pEGFP-c1 and expressed in 293T cells through transfection, where the GFP-tagged mRNF146 construct was transfected as a positive control. The level of endogenous PAR induction by overexpressing hRNF146 was 6-7 folds lower than that caused by mRNF146 or its WWE domain (Figure 5b). The difference is therefore likely due to the region outside the conserved RING and WWE domains.

The nature of induction in PAR levels by RNF146 is not known. One hypothesis is that such induction could be partially due to elevated levels of PARylated cellular proteins. On the other hand, however, overexpression of ubiquitin E3 ligase RNF146 should result in a decrease in levels of PARylated proteins, in particularly PARdU substrates, thus reducing overall cellular PARylation level. In order to test the conflicting ideas, we chose to examine endogenous Tankyrase 1 & 2 (TNKS1/PARP5a and TNKS2/PARP5b) because they are continually auto-PARylated in cells (Callow et al., 2011) as well as the fact that they are known PARdU substrates of RNF146. To our surprise, analysis by western blot revealed that cells overexpressing mRNF146 or its WWE domain, compared to those expressing hRNF146, had elevated levels of TNKS 1

& 2 (Figure 5c). In addition, the levels of increase in the amount of PARylated TNKS proteins were comparable in cells expressing full-length mRNF146 or its WWE domain. It seems that overexpression of mRNF146 resulted in a stabilization of PARylated TNKS proteins, similar to overexpression of mRNF146 WWE domain, rather than enhancing protein degradation. It was also possible, however, the increased signals of TNKS 1 & 2 detected on western blots could be purely due to a stabilization of attached PAR chains on PARylated proteins rather than a change in amounts of proteins. As a result, in the following content of this thesis, the term "increased levels of PARylted TNKS 1 & 2" is used referring to elevated TNKS signals detected on western blots caused by either of the two mechanisms until further experiments could distinguish them apart in the near future.

(Next page) Figure 5 | Overexpression of hRNF146 leads to lower levels of PAR-induction compared to mRNF146. a) Protein sequence alignment between hRNF146 (labeled in green) and mRNF146 (labeled in red). Regions for RING and WWE domains are highlighted. b) Western blot of cell lysates from 293T cells expressing GFP-tagged hRNF146, mRNF146 and mRFN146 WWE domain using antibodies against PAR (left) and GFP (right). c) Western blot of the same cell lysates using antibodies against TNKS 1 & 2.

a

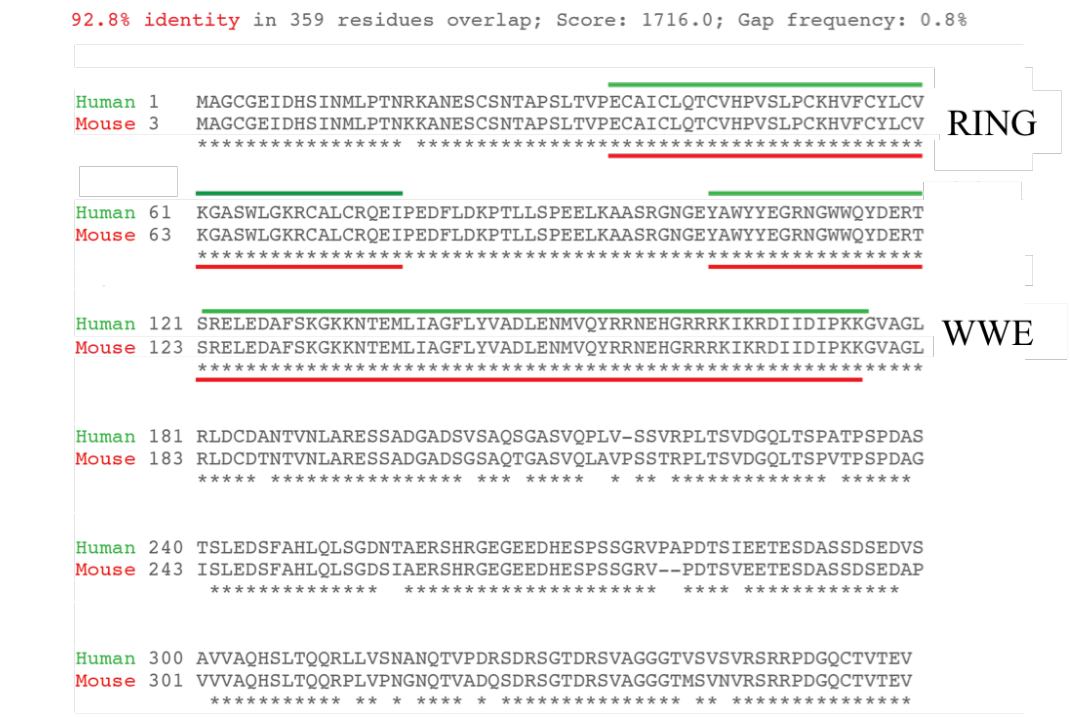
92.8% identity in 359 residues overlap; Score: 1716.0; Gap frequency: 0.8%
Human 1 MAGCGEIDHSINMLPTNRKANESCSNTAPSLTVPECAICLQTCVHPVSLPCKHVFCYLCV
Mouse 3 MAGCGEIDHSINMLPTNKKANESCSNTAPSLTVPECAICLQTCVHPVSLPCKHVFCYLCV
RING
Human 61 KGASWLGKRCALCRQEIPEDFLDKPTLLSPEELKAASRGNGEYAWYYEGRNGWWQYDERT
Mouse 63 KGASWLGKRCALCRQEIPEDFLDKPTLLSPEELKAASRGNGEYAWYYEGRNGWWQYDERT
Human 121 SRELEDAFSKGKKNTEMLIAGFLYVADLENMVQYRRNEHGRRRKIKRDIIDIPKKGVAGL
Mouse 123 SRELEDAFSKGKKNTEMLIAGFLYVADLENMVQYRRNEHGRRRKIKRDIIDIPKKGVAGL
WWE
Human 181 RLDCDANTVNLARESSADGADSVSAQSGASVQPLV-SSVRPLTSVDGQLTSPATPSPDAS
Mouse 183 RLDCDTNTVNLARESSADGADSGSAQTGASVQLAVPSSTRPLTSVDGQLTSPVTPSPDAG
Human 240 TSLEDSFAHLQLSGDNTAERSHRGEGEEDHESPSSGRVPAPDTSIEETESDASSDSEDVS
Mouse 243 ISLEDSFAHLQLSGDSIAERSHRGEGEEDHESPSSGRV--PDTSVEETESDASSDSEDAP
Human 300 AVVAQHSLTQQRLLVSNANQTVPDRSDRSGTDRSVAGGGTVSVSVRSRRPDGQCTVTEV
Mouse 301 VVVAQHSLTQQRPLVPNGNQTVADQSDRSGTDRSVAGGGTMSVNVRSRRPDGQCTVTEV

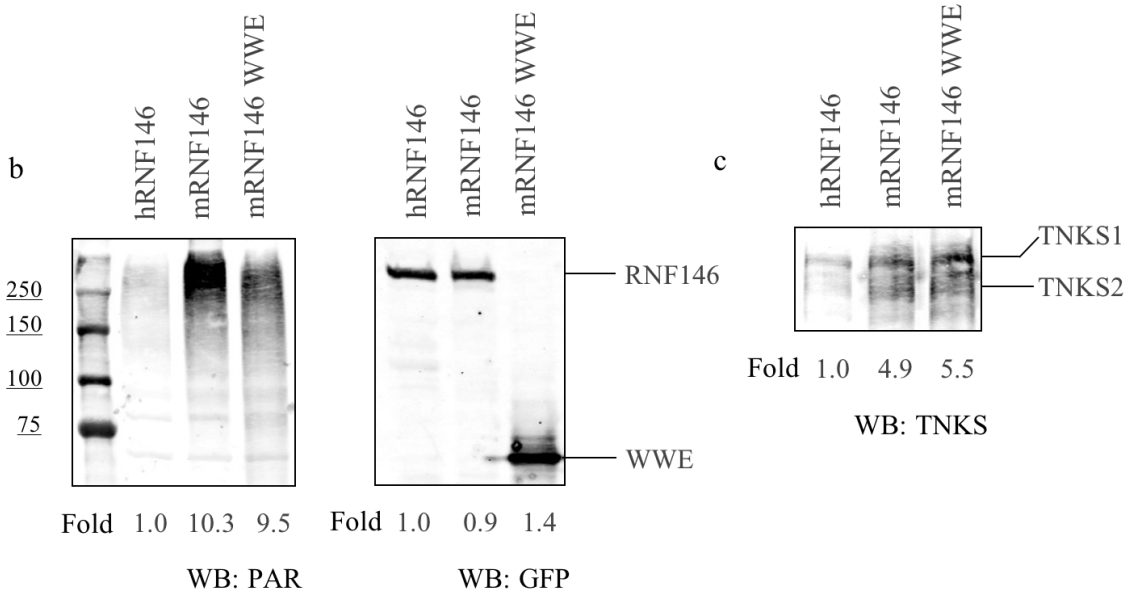
b
hRNF146
mRNF146
mRNF146 WWE
250
150
100
75
RNF146
WWE
Fold 1.0 10.3 9.5
Fold 1.0 0.9 1.4
WB: PAR
WB: GFP
c
hRNF146
mRNF146
mRNF146 WWE
TNKS1
TNKS2
Fold 1.0 4.9 5.5
WB: TNKS

Overexpression of RNF146 WWE domain alone is sufficient to increase endogenous PAR levels

Our analyses found that overexpression of the mRNF146 WWE domain alone was sufficient to increase the endogenous PAR levels although the pattern of PAR induction was slightly different from that caused by overexpressing full-length mRNF146. Nonetheless, the expression of full-length hRNF146 had a more limited effect on PARylation despite 100% conservation of the WWE domain. We hypothesize that the regions outside of the hRNF146 WWE domain negatively regulates the induction on PAR levels when full-length hRNF146 is expressed in cells. To further analyze the regions of hRNF146 responsible for affecting PAR levels, various protein fragments of hRNF146 were cloned into pEGFP-c1 vectors (Figure 6). GFP-tagged recombinant proteins were overexpressed in 293T cells for 24 h after transfection. Cell lysates were collected and analyzed on western blot. As we expected, overexpression of the GFP-tagged human RNF146 WWE domain alone was able to increase cellular PARylation levels (Figure 7a). In contrast, addition of other regions (RING–WWE or WWE–Cter) did not increase PAR levels.

To determine whether the differences in effects on PARylation could be due to different expression levels of RNF146 protein fragments, a dose-dependent transfection assay was performed. Expressing the hRNF146 WWE domain increased endogenous PAR levels as the expression levels increased, whereas expressing varying levels of full-length hRNF146 failed to achieve a similar effect (Figure 8).

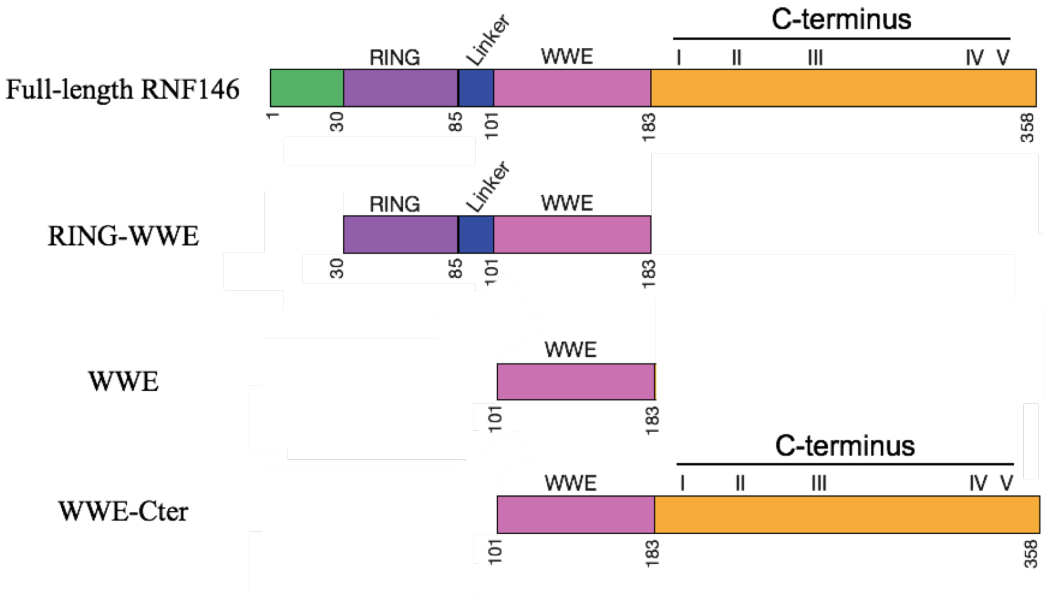

Figure 6 | Diagram for full-length hRNF146 and its truncated protein fragment constructs. The RING domain (30-85) is highlighted in purple and WWE domain (101-183) is highlighted in pink. The C-terminus region is highlighted in yellow with roman numerals indicating potential TNKS interacting sites.

(Next pages) Figure 7 | Overexpression of hRNF146 WWE domain is sufficient to increase cellular levels of PAR as well as TNKS 1 and 2. a) Western blot of cell lysates from 293T cells over-expressing GFP, GFP-tagged full-length hRNF146 and hRNF146 protein fragments (RING–WWE, WWE, WWE-Cter) using antibodies against PAR (left) and GFP (right). According to manufacturer's protocol, the PAR antibody cross-reacts with bovine serum albumin (left, 66 kDa) from the cell medium. (The same situation applies to all following western blots against PAR staining) b) Western blot of the same cell lysates using antibody against TNKS 1 and 2.

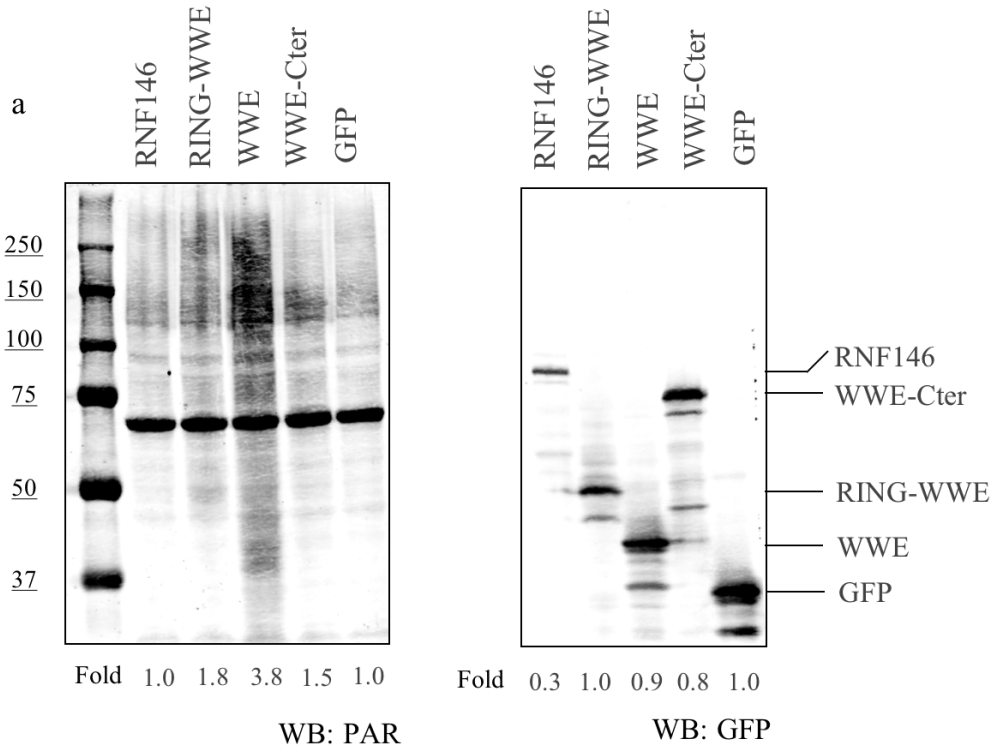
a
RNF146
RING-WWE
WWE
WWE-Cter
GFP
250
150
100
75
50
37
Fold 1.0 1.8 3.8 1.5 1.0
WB: PAR
Fold 0.3 1.0 0.9 0.8 1.0
WB: GFP
RNF146
WWE-Cter
RING-WWE
WWE
GFP

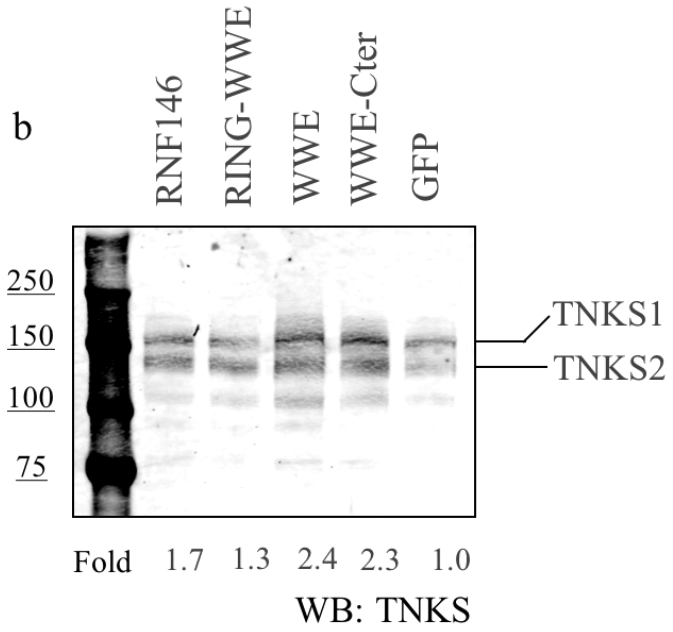
b
RNF146
RING-WWE
WWE
WWE-Cter
GFP
250
150
100
75
TNKS1
TNKS2
Fold 1.7 1.3 2.4 2.3 1.0
WB: TNKS

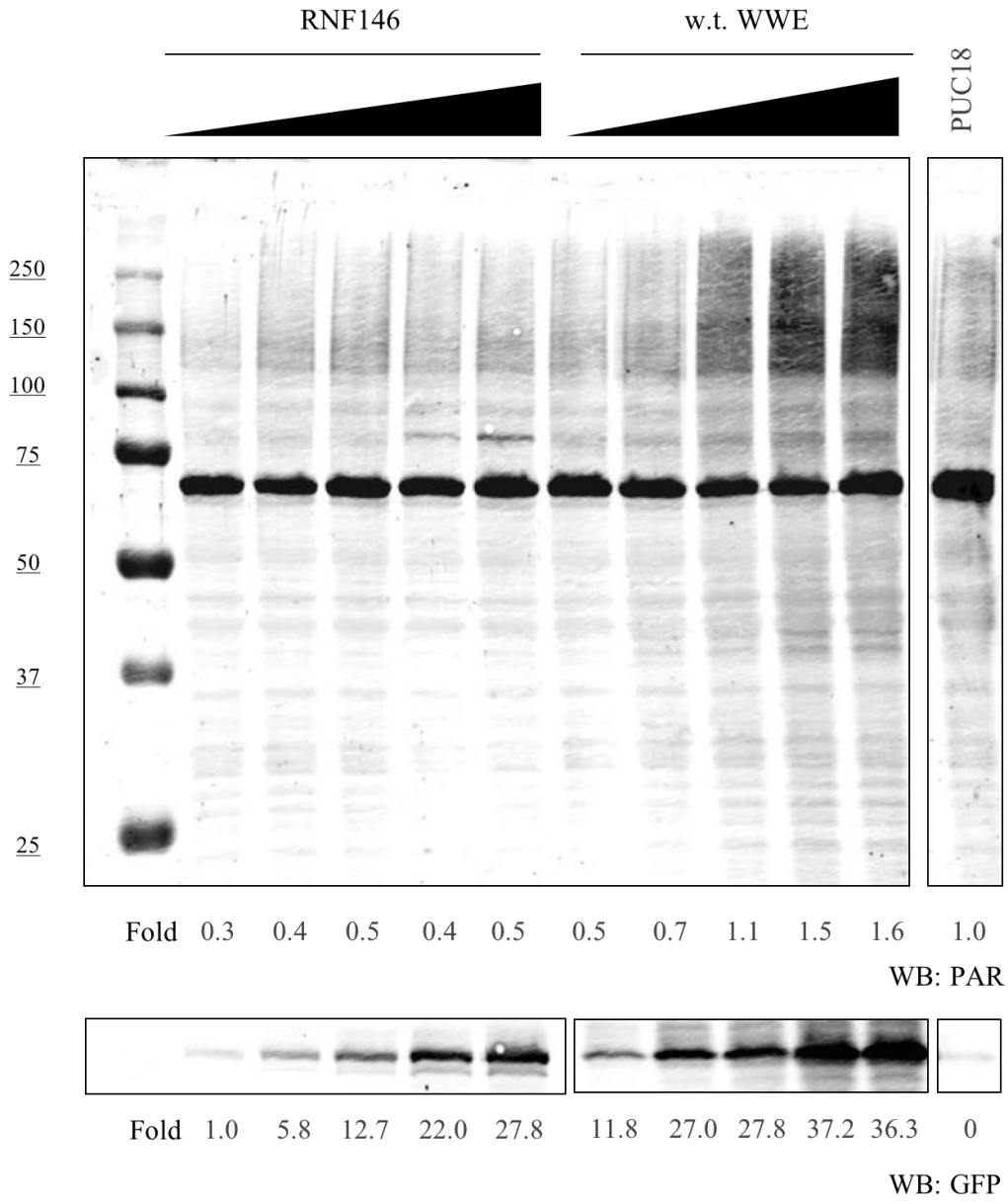

Figure 8 | Overexpression of wild-type hRNF146 WWE domain but not full-length hRNF146 increases endogenous PAR level in a dose-dependent manner. Western blot of cell lysates from 293T cells over expressing GFP-tagged RNF146 and its WWE domain using antibody against PAR (top) and GFP (bottom). pUC18 plasmid was transfected in 293T cells as the negative control and the blot was exposed under the same parameters.

Again, we examined the endogenous levels of TNKS 1 & 2. Compared to cells expressing hRNF146, hRNF146 RING-WWE and GFP, overexpression of the hRNF146 WWE domain as well as the WWE–Cter construct increased levels of PARylated TNKS 1 & 2 in cells (Figure 7b). Notably, overexpression of WWE–Cter increased the total PARylated TNKS 1 & 2 levels without necessarily inducing the endogenous PAR level. One potential explanation is that the Cter region is known to contain five Tankyrase binding motifs (DaRosa et al., 2015); thus, overexpression of WWE–Cter might potentially stabilize the interaction, resulting in an increase in TNKS 1 & 2 levels.

As mentioned above, PARylated TNKS 1 & 2 were targets of RNF146 (as well as the RNF146 RING–WWE fragment) ubiquitin E3 ligase activity (Callow et al., 2011). We reasoned that overexpressing hRNF146 with impaired E3 activity in cells could further result in elevated levels of PARylated TNKS 1 & 2 compared to expressing wild-type hRNF146 in cells. As a result, site-directed mutagenesis was conducted to change the Lys61 residue to Ala (See also Introduction). Mutations at the Lys61 residue in the RNF146 RING domain uncouples its ubiquitin E3 ligase activity from the PAR-binding ability of WWE domain; the mutant exhibits constitutive basal E3 ligase activity as binding of PAR polymers cannot activate the RING domain (DaRosa et al., 2015; See also Introduction). As expected, overexpression of human RNF146 K61A mutant showed a higher induction in PARylated TNKS 1 & 2 levels than the levels induced by wild-type RNF146 (Figure 9). Moreover, basal E3 activity potentially explains the difference in TNKS levels induced by overexpressing the WWE domain and by overexpressing

RNF146 K61A mutant. Whether the increase in PARylated TNKS1 and 2 is part of an increase in endogenous PAR levels will be followed up in the future.

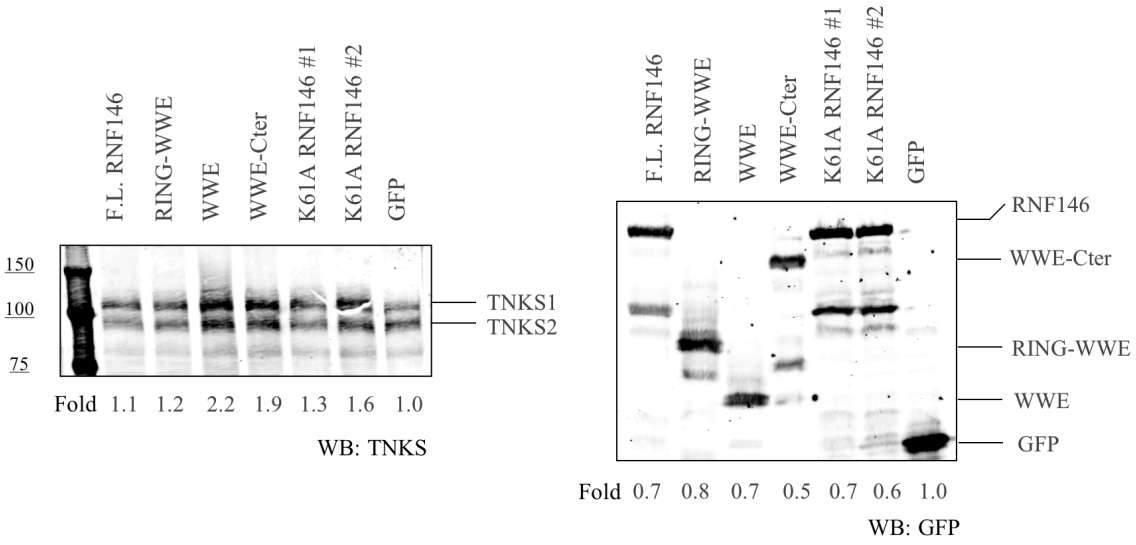

Figure 9 | Mutations in the RING domain lowers the level of TNKS 1 & 2 induction caused by overexpressing hRNF146. Western blot of cell lysates from 293T cells overexpressing GFP-tagged RNF146, its protein fragments (RING–WWE, WWE, WWE–Cter) and the mutant (K61A) in 293T cells. K61A RNF146 #1 and #2 were cloned constructs from two bacterial clones.

PAR induction by hRNF146 WWE is dependent on high affinity binding to iso-ADPr

Given that the primary function of the RNF146 WWE domain is to bind to *iso*-ADPr, we tested if its affinity toward PAR correlates with levels of PAR induction detected on western blots. A mutation changing Gln153 to Ala in the hRNF146 WWE domain impairs its affinity to *iso*-ADPr (Figure 2b). The GFP-tagged hRNF146 Q153A WWE domain was overexpressed in 293T cells along with the wild-type WWE domain as the positive control (Figure 10). PAR levels increased in a dose-dependent manner with increasing expression of the wild-type WWE domain but not with the Q153A mutant. In fact, endogenous PAR levels in cells expressing the Q153A mutant were equivalent to those in negative control cells (transfected with the pUC18 plasmid) –an induction in PARylated TNKS levels was once again detected by overexpressing wild-type WWE but not the Q153A mutant. To investigate whether the hRNF146 WWE has a general effect on increasing PARylation of all PARylated proteins we also probed for PARP1—a well-established target that is PARylated upon DNA damage. Both the protein levels and PARylation levels of PARP1 remained the same across the samples (Figure 11), suggesting that overexpression of the RNF146 WWE domain only increases the level of specific PARylated targets and/or targets that are PARylated in the basal condition.

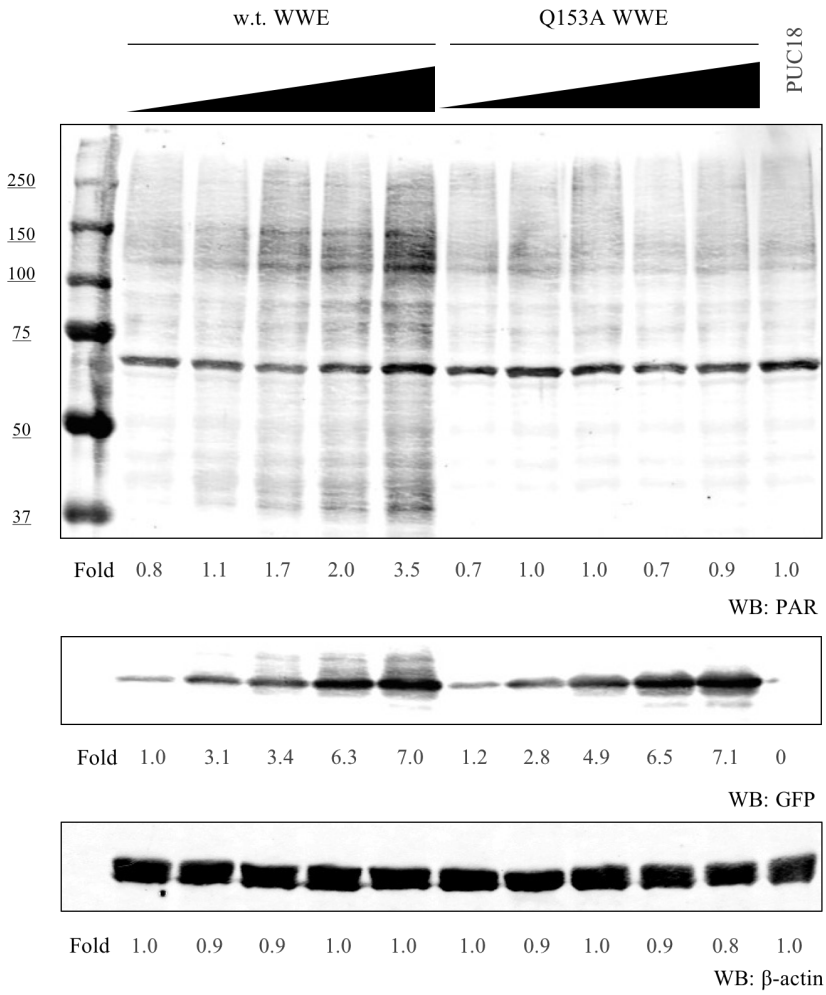

Figure 10 | Mutation reducing PAR binding affinity impairs cellular PAR induction by hRNF146 WWE domain. Western blot of cell lysates from 293T cells over expressing GFP-tagged wild-type hRNF146 WWE domain and PAR-binding deficient mutant Q153A WWE domain using antibody against PAR (top), GFP (middle) and β-actin (bottom).

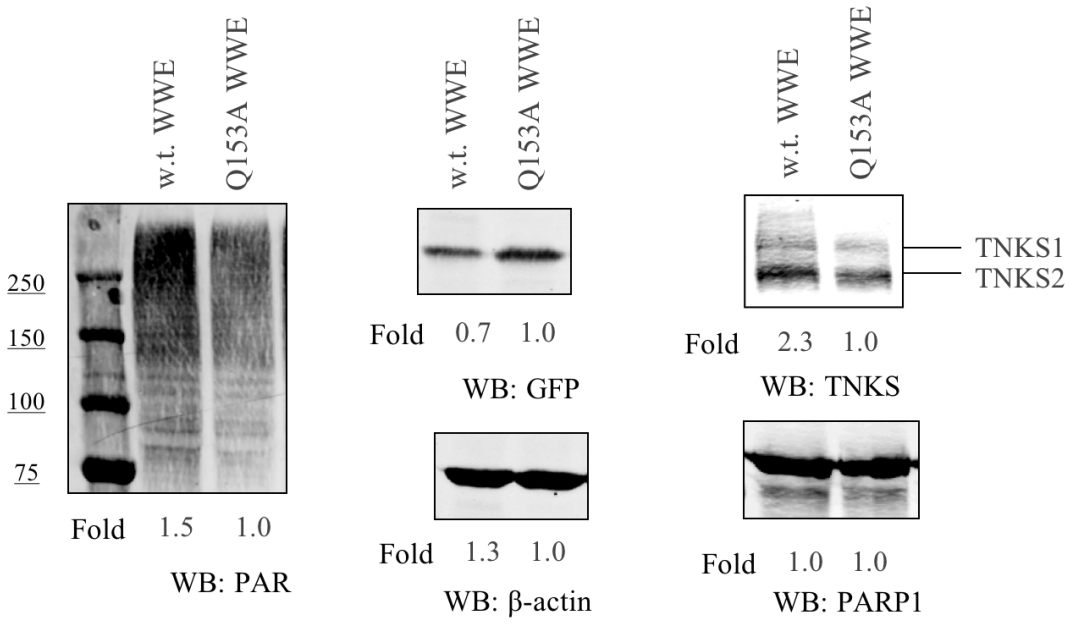

Figure 11 | Mutations that reduce PAR binding affinity impair TNKS 1 & 2 but not PARP1 induction levels by hRNF146 WWE domain. Western blot of cell lysates from 293T cells over expressing GFP-tagged wild-type hRNF146 WWE domain and PAR-binding deficient mutant Q153A WWE domain using antibody against PAR (left), TNKS 1 and 2, GFP, β-actin and PARP1 (right, from top to bottom).

To further examine the correlation between PAR-binding affinity and PAR-induction ability of RNF146 WWE domain, additional PAR-binding-deficient WWE mutants were generated by site-directed mutagenesis. Previous ITC data suggested that Y144A and R163A mutants showed no detectable interactions with *iso*-ADPr *in vitro* (Figure 2b). Expressing these WWE mutants in 293T cells led to negligible PAR inductions even though the same relative amounts of each expressed protein were detected compared to the wild-type WWE domain (Figure 12a). Consistently, no TNKS 1 & 2 induction was identified among cells expressing these mutants (Figure 12b).

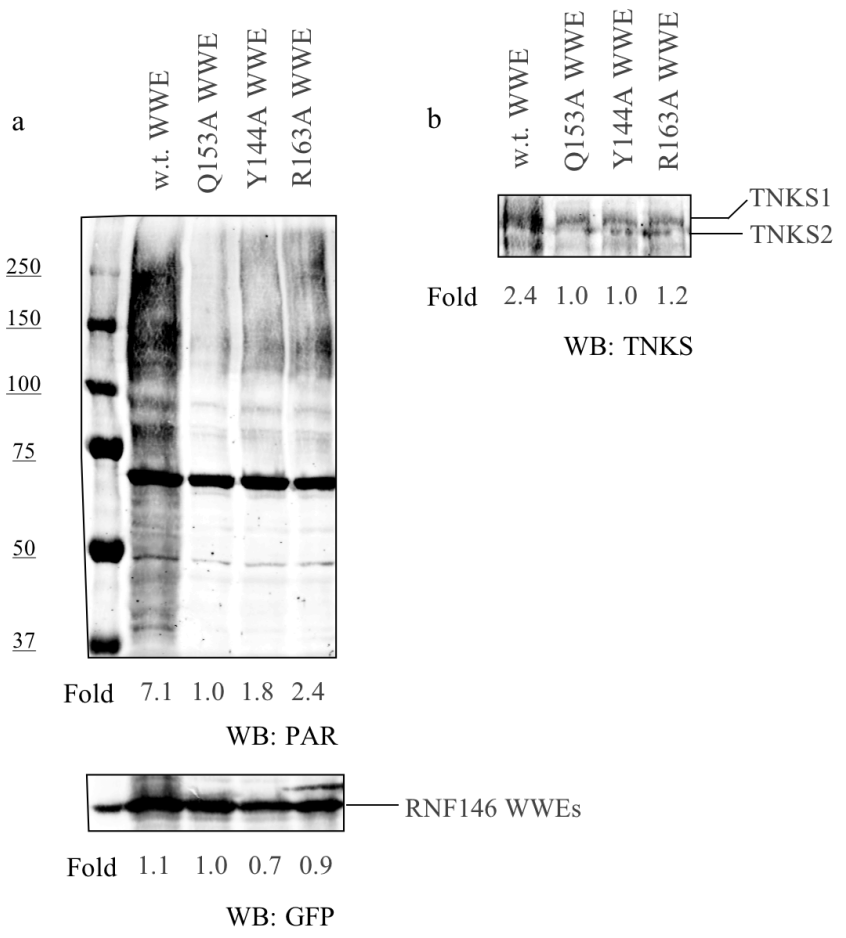

Figure 12 | Mutations that reduce PAR affinity of RNF146 WWE domain impairs level of PAR/TNKS 1 & 2 upon overexpression. Western blot of cell lysates from 293T cells overexpressing GFP-tagged wild-type (w.t.) RNF146 WWE domain and its PAR-binding deficient mutants in 293T cells using antibodies against PAR (a, top), GFP (a, bottom), TNKS 1 & 2 (b).

PAR induction by overexpressing the RNF146 WWE domain in multiple cell lines.

As the data presented above were generated with the 293F or 293T cell lines, we tested a similar dose-dependent transfection procedure in both HeLa and DLD1 cells to determine if the results could be reproduced in other cell lines. While an increase in cellular PAR levels was indeed observed after overexpressing the wild-type RNF146 WWE domain in both cell lines, PAR signals detected on western blot from DLD1 cell lysates were much weaker than PAR signals from 293F/T and HeLa (Figures 13 and 14). Low transfection efficiency in DLD1 cells (less than 20% of the total cells, data not shown) could be a possible explanation for the weaker induction of PAR signals.

(Next page) Figure 13 | Overexpressing hRNF146 WWE domain induces cellular PAR in HeLa cells. Western blot of cell lysates from HeLa cells over expressing GFP-tagged wild-type hRNF146 WWE domain and PAR-binding deficient mutant Q153A WWE domain using antibody against PAR (top), GFP (bottom).

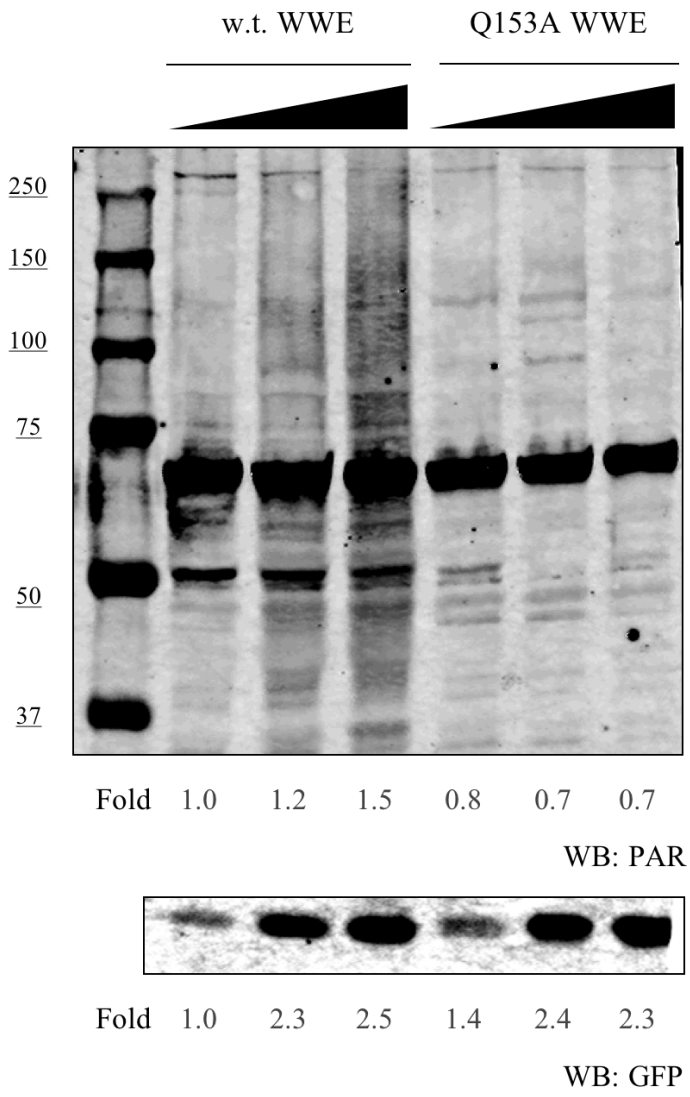
w.t. WWE
Q153A WWE
250
150
100
75
50
37
Fold 1.0 1.2 1.5 0.8 0.7 0.7
WB: PAR
Fold 1.0 2.3 2.5 1.4 2.4 2.3
WB: GFP

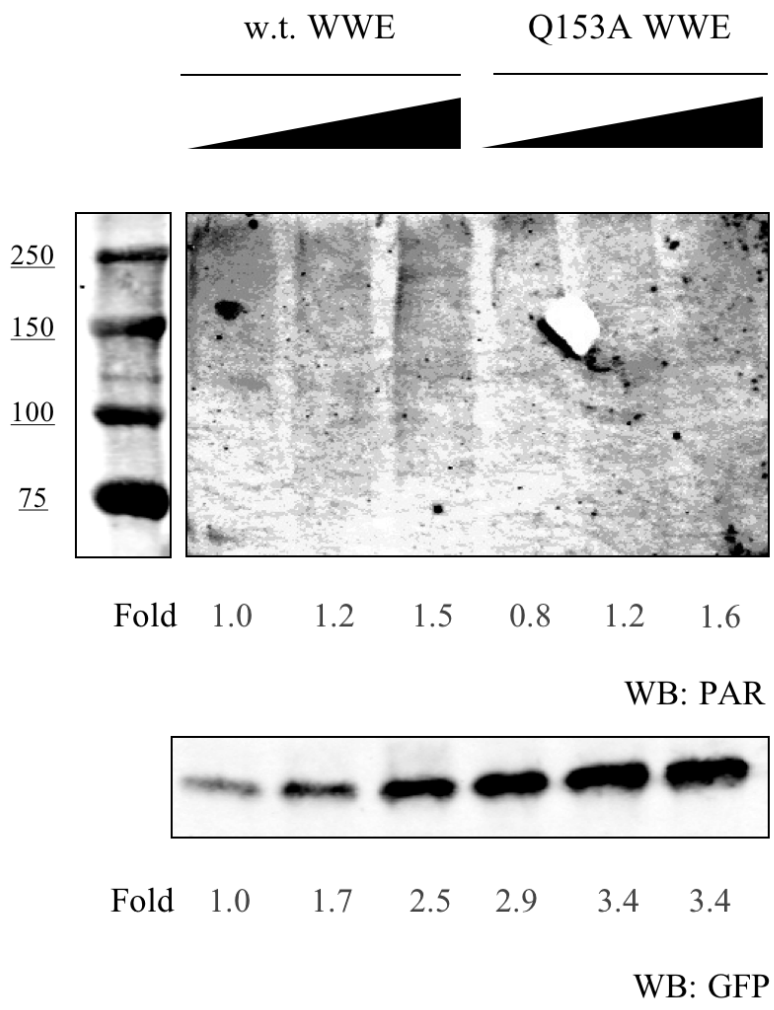

Figure 14 | Overexpressing hRNF146 WWE domain induces cellular PAR in DLD1 cells. Western blot of cell lysates from DLD1 cells over expressing GFP-tagged wild-type hRNF146 WWE domain and PAR-binding deficient mutant Q153A WWE domain using antibody against PAR (top), GFP (bottom).

Overexpression of the wild-type RNF146 WWE domain but not the mutant leads to puncta formation in cells

Limited transfection efficiency as well as low protein expression in both HeLa and DLD1 cells led us to explore if results could be observed on a single-cell scale so that any significant effect would not be underestimated by untransfected cells. HeLa cells were chosen for further examination because of its moderate expression of GFP-tagged recombinant proteins. After transfections, cells were fixed on slides for immunostaining and visualized by fluorescence microscopy. Overexpression of the GFP-tagged wild-type RNF146 WWE domain led to a formation of individual puncta in the cytoplasm of HeLa cells (Figure 15, GFP channel). Co-staining with anti-PAR antibodies revealed co-localization between endogenous PAR and the GFP-tagged RNF146 WWE domain (Figure 15, Merged channel), compared to diffuse pattern of PAR observed in untransfected cells. Additionally, expressing GFP (data not shown) or the GFP-tagged RNF146 WWE Q153A mutant failed to produce any visible puncta (Figure 15). Thus, puncta formation correlated with the PAR-binding affinity of the RNF146 WWE domain. However, puncta were not detected in all cells expressing the GFP-tagged RNF146 WWE domain, suggesting that other factors, such as cell cycle stage, could contribute to their formation.

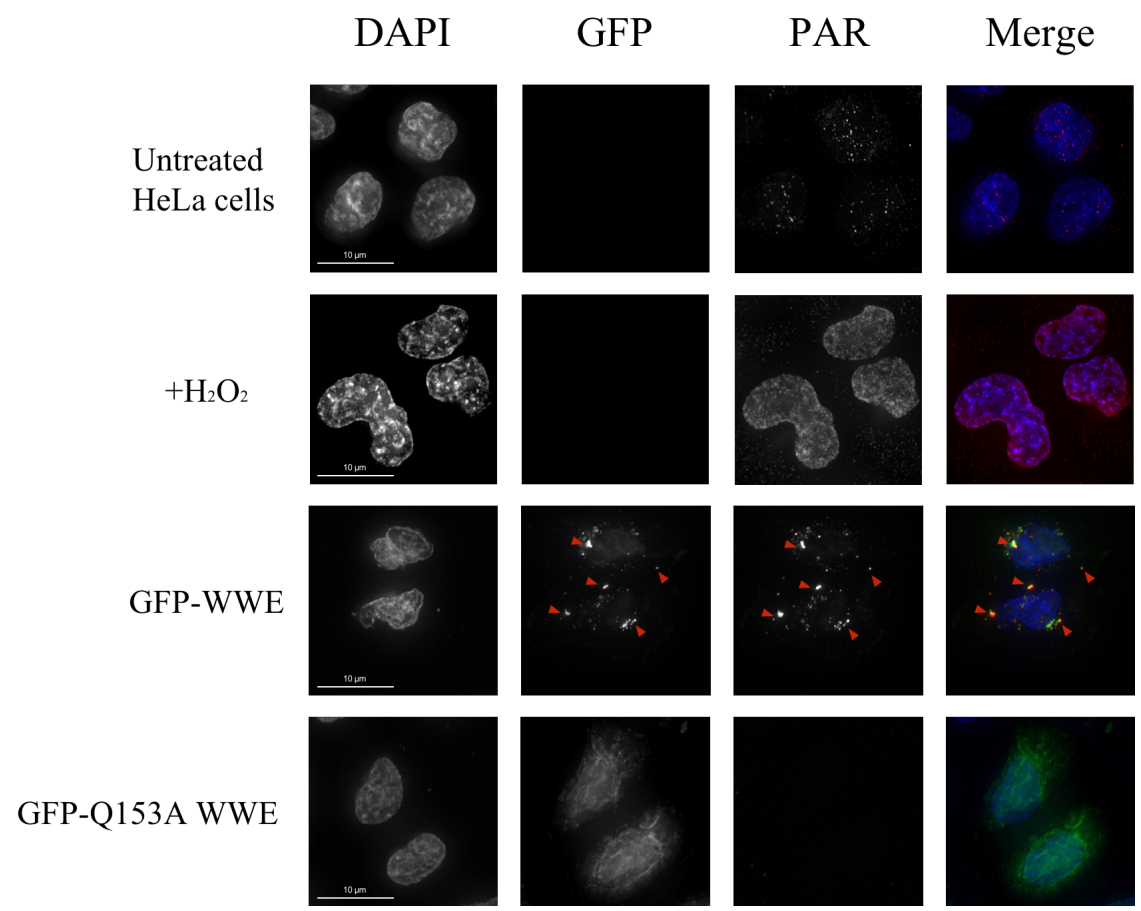

Figure 15 | Wild-type RNF146 WWE domain induces formation of PAR-rich puncta in cells. Untransfected HeLa cells (first row) were treated with 1 µM hydrogen peroxide for 10 minutes to induce detectable PAR staining (second row). Immunofluorescence microscopy images of HeLa cells expressing either GFP-tagged wild-type RNF146 WWE domain (third row) or PAR-binding deficient mutant Q153A WWE domain (bottom row) using antibodies against PAR.

Martino-Echarri et al. (2016A) previously reported the formation of axin-rich puncta after TNKS 1/2 inhibition. Their model suggested that PARP inhibitor treatments caused aggregation of the Axin1-TNKS 1 & 2 complex, which led to formation of visible puncta in cells. Thus, we looked for a similar mechanism in the formation of puncta in

cells overexpressing the RNF146 WWE domain. We found that GFP-tagged wild-type RNF146 WWE co-localized with TNKS 1 & 2 (Figure 16a). We have yet to verify whether or not Axin1 co-localizes with these loci. In addition, we also investigated whether the puncta were part of stress granules by immunostaining with antibodies to eIF3 (Kedersha et al., 2001). Co-localization with eIF3 was not detected, indicating that the puncta were not part of stress granules (Figure 16b, c).

(Next page) Figure 16 | Wild-type RNF146 WWE domain co-localizes with TNKS 1 & 2, but not the stress granule marker eIF3. Immunofluorescence microscopy images of HeLa cells expressing either GFP-tagged wild-type RNF146 WWE domain or PAR-binding deficient mutant Q153A WWE domain using antibodies against TNKS 1 & 2 (a) and eIF3 (b). Untransfected HeLa cells were treated with 250 μM sodium arsenite for 30 minutes to induce eIF3 localization to stress granules (c).

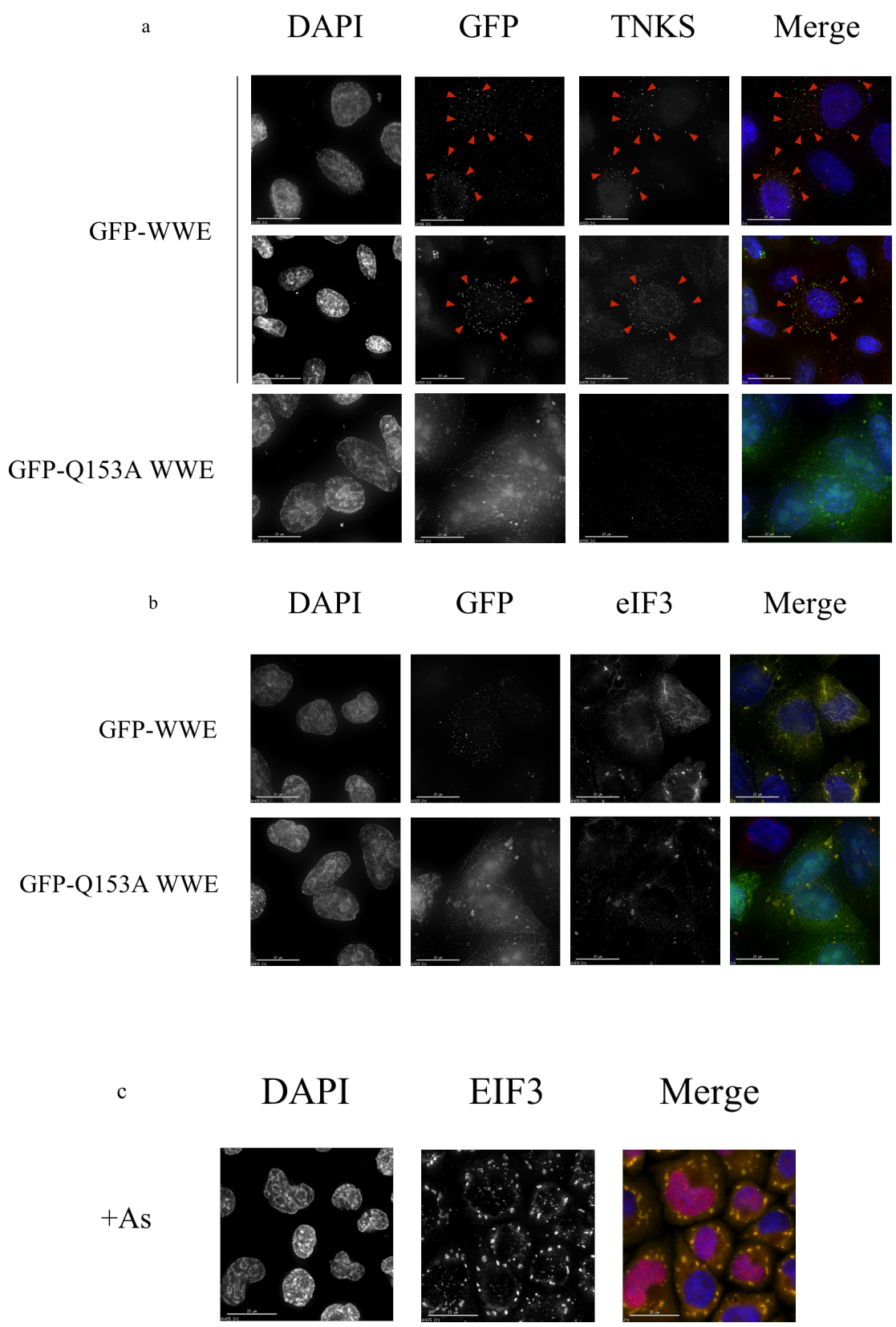
a
DAPI
GFP
TNKS
Merge
GFP-WWE
GFP-Q153A WWE
b
DAPI
GFP
eIF3
Merge
GFP-WWE
GFP-Q153A WWE
c
DAPI
EIF3
Merge
+As

Discussion

In this thesis, we report a novel phenomenon of RNF146 and its WWE domain. Overexpression of RNF146 and the WWE domain in cells increases endogenous PAR levels detected by western blots and immunofluorescence microscopy. We also showed that this increase in cellular PAR levels was partially due to the elevated levels of certain PARylated proteins, such as TNKS 1 & 2. Moreover, the level of PAR induction was tightly linked with the PAR-binding affinity of the RNF146 WWE domain. Although both mouse and human RNF146 WWE domains were capable of increasing endogenous PAR levels to a similar extent, overexpression of two full-length RNF146 proteins showed different PAR profiles detected on western blot. At the same time, the distinct levels of PARylated TNKS 1 & 2 induction by mouse and human RNF146 were also observed. The major differences in primary protein sequences of mouse and human RNF146 lie in the N-terminus as well as the C-terminal region downstream of their WWE domains. As mentioned above, potential TNKS-interacting motifs lie at the C-terminus of the RNF146 protein. Whether interaction between the RNF146 C-terminus and TNKS 5ARC domain is a requirement for TNKS degradation through ubiquitination and whether the differences in C-terminus between mouse and human RNF146 affect the levels of PAR/TNKS induction are questions worth exploring in the near future.

Consistent results of PAR induction by RNF146 WWE domain overexpression have driven our curiosity toward the molecular mechanism behind this phenomenon. Although we cannot exclude the possibility that overexpressing the RNF146 WWE domain could directly or indirectly boost formation of new PAR polymers, we favor the idea that interaction between the WWE domain and PARylated proteins prevents removal

of PAR chains by hydrolases and blocks protein degradation by endogenous enzymes, such as PAR-dependent ubiquitin E3 ligases. As a result, a prolonged life span of PARylated proteins has been translated into elevated PAR levels revealed on western blot.

We also illustrated the formation of TNKS-rich puncta in the cytosol by overexpressing the RNF146 WWE domain. Moreover, our data also indicated the possible presence of PARylated TNKS proteins within the puncta induced by overexpressing the RNF146 WWE domain, as demonstrated by the following evidence: First, expressing a PAR-binding deficient mutant, the RNF146 Q153A WWE domain, failed to generate visible puncta in cells. Second, expressing the wild-type WWE domain in the mitochondria also inhibits puncta formation, which is likely due to the spatial separation between the WWE domain and TNKS proteins (See below, Figure 19).

In addition, another study revealed that overexpressing the TNKS proteins or inhibiting TNKS activities facilitated assembly of TNKS-rich puncta in cells. Meanwhile, removing or mutating the sterile alpha motif (SAM) domain, a domain that facilitates self-oligomerization of TNKS proteins, inhibits visible puncta formation caused by overexpression (De Rycker and Price, 2004). In addition, auto-PARylations of TNKS proteins have been shown to increase protein solubility by preventing self-oligomerization *in vitro* (DaRosa et al., 2016). All the evidence suggests that PARylation inhibits TNKS oligomerization and leads to a change in protein solubility. How overexpression of RNF146 WWE promotes formation of TNKS-containing pucta while potentially stabilizing its PARylation is the question we would like to pursue in the near future.

RNF146 WWE domain as a potential tool for modulating endogenous PARylation levels in different subcellular compartments

As mentioned in the Introduction, due to different localizations of PARPs, PARylation events in each subcellular compartment could lead to a distinct physiological significance for normal cellular activities. Thus, modulating subcellular PARylation could be useful for further identifying different aspects of PARylation in cells. Induction in endogenous PAR levels by overexpressing the RNF146 WWE domain has led us to explore the possibility of artificially altering endogenous PARylation in different cellular compartments.

First, we investigated the relative strength of PAR induction by the RNF146 WWE domain. A simple comparison was performed between the level of PAR increase by PARG inhibition and by RNF146 WWE overexpression. Transfected cells were treated with or without a membrane-permeable PARG inhibitor (a gift from Dr. Ian Waddell, Cancer Research UK, Manchester) for 2 h before harvesting. Compared with cells expressing the wild-type RNF146 WWE domain (without PARG inhibitor treatment), untransfected cells treated with the PARG inhibitor showed a similar level but distinct pattern of PAR signals (Figure 17). PARG treatment with WWE-expressing cells led to an even higher level of PAR increase. PARG inhibition is known to cause a global increase in cellular PAR; but effective as it is, PARG inhibition is detrimental to cells (Stowell et al., 2016). In contrast, the RNF146 WWE domain may provide a way to fine-tune the dynamics between PARylation and de-PARylation of proteins.

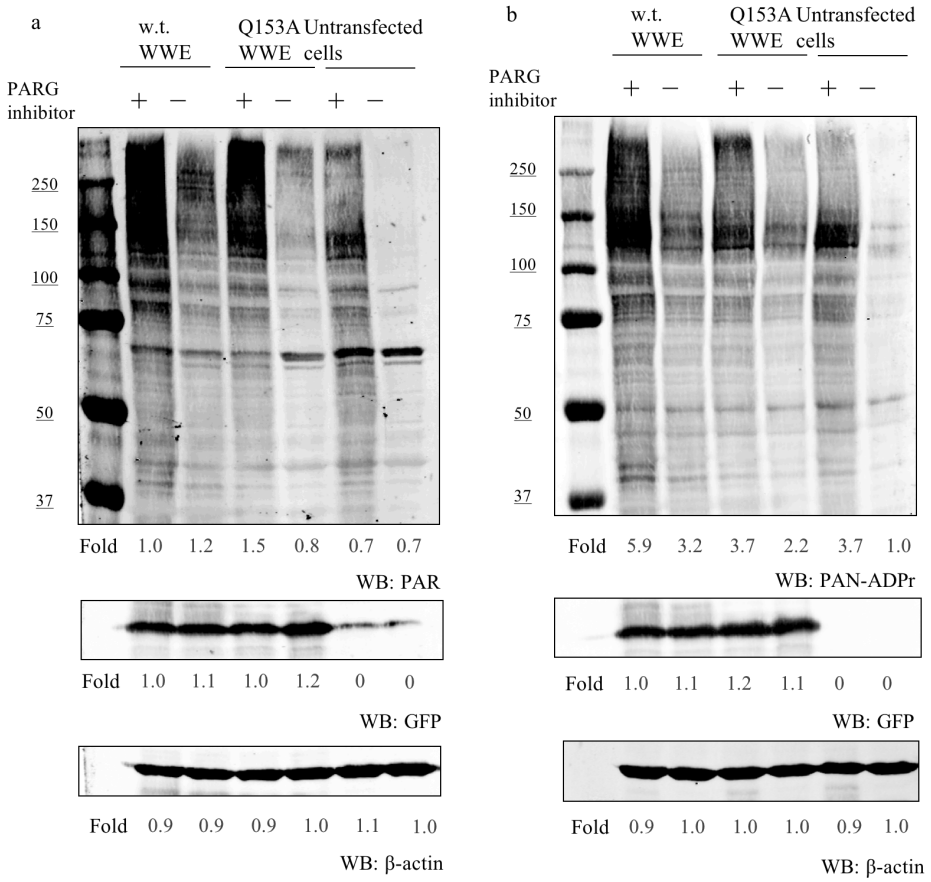

Figure 17 | Overexpression of hRNF146 WWE domain mimics cellular PAR induction by PARG inhibition. a) Western blot of cell lysates from 293T cells overexpressing GFP-tagged RNF146 WWE domains and PAR-binding deficient mutant Q153A WWE domain with/without PARG inhibitor treatment, using antibody against PAR (top), GFP (middle) and β-actin (bottom). b) Western blot of the same cell lysates using antibody against PAN-ADPr (top), GFP (middle) and β-actin (bottom).

Next, we checked if RNF146 is the best candidate for PAR induction among the WWE domain family. DNA sequences of different WWE domains were cloned into pEGFP-c1 and expressed in 293T cells. Expressing the RNF146 WWE domain led to the strongest PAR induction, as previously observed. Several PARP WWE domains showed weak or no PAR increase in general (Figure 18). To date, overexpressing the RNF146 WWE domain demonstrated the strongest PAR induction. PARP 7 WWE domain and other E3 ligase WWE domains will be tested in the future.

(Next page) Figure 18 | Overexpressing WWE domains from various PARPs showed negligible PAR induction compared to RNF146 WWE domain. Western blot of cell lysates from 293 T cells over-expressing GFP-tagged WWE domains in 293T cells using antibodies against PAR (left) and GFP (right). The "PAPR12 WWE 1" and "PARP12 WWE 2" refer to GFP-tagged recombinant proteins containing either PAPR12 WWE domain. The "PAPR12 WWE (both)" refer to GFP-tagged recombinant protein containing both PAPR12 WWE domains.

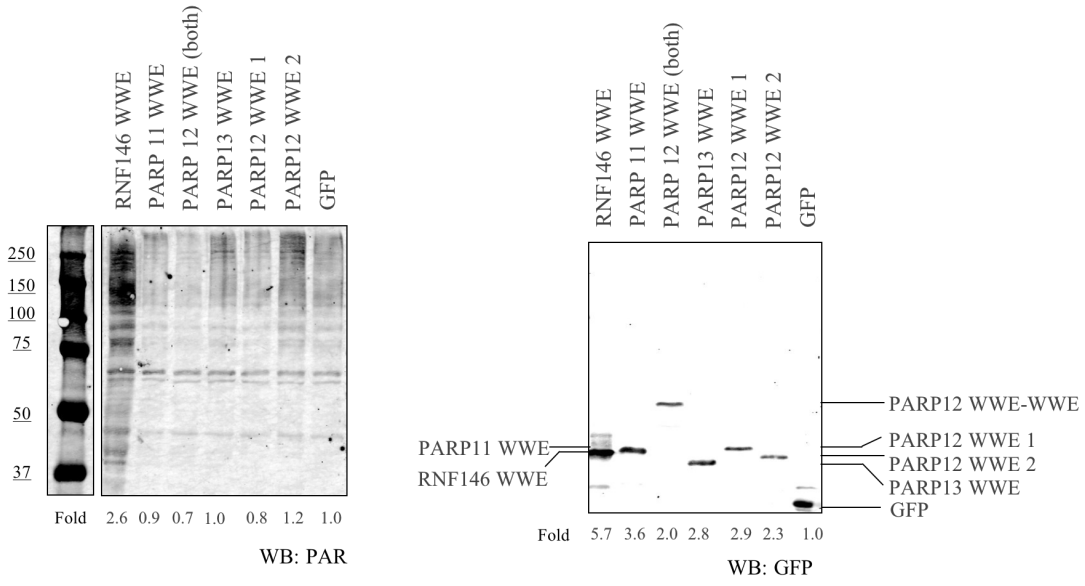

By attaching different localization signals, we transported the GFP-tagged RNF146WWE domain into subcellular compartments and visualized them by fluorescence microscopy. A mitochondrial-matrix-targeting peptide sequence subunit 9 (Su9) of the F0-ATPase, was attached to the N-terminus of the WWE domain while the GFP sequence was fused to the C-terminus (Haucke et al., 1995). Expressing the Su9-WWE-GFP recombinant protein in HeLa cells resulted in a distinct pattern of distribution in the cytoplasm (Figure 19). Immunostaining against PDH, a mitochondrial marker, further confirmed the correct localization of the Su9-WWE-GFP protein to mitochondria (data not shown). However, we were not able to detect any visible puncta formed by the Su9-WWE-GFP protein; neither did we see any co-localization between PAR and GFP signals as seen for the untargeted WWE construct. Our data are consistent with the absence of any PARPs identified in mitochondria.

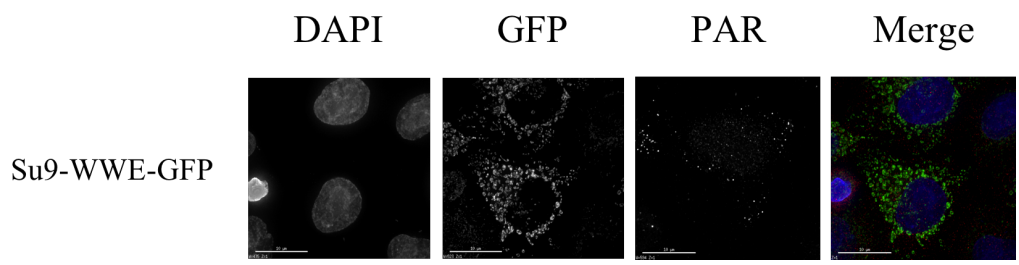

Figure 19 | Targeting RNF146 WWE domain into Mitochondrial matrix inhibits formation of PAR-rich puncta in the cytoplasm. Immunofluorescence microscopy images of HeLa cells expressing GFP-tagged RNF146 WWE domain in mitochondrial matrix using antibody against PAR.

Along with exploring the potential for developing the RNF146 WWE domain as a general tool for modulating cellular PAR levels, several questions remain unanswered. First, it is still unclear whether the RNF146 WWE domain shows any binding specificity bias toward PARylated proteins. The crystal structure of RNF146 WWE domain-binding *iso*-ADPr provided the theoretical basis for its potential interaction with the majority of PARylated proteins in cells. In addition, the recombinant RNF146 WWE domain is available commercially as a reagent for detecting cellular PARylation. However, no systematic study has been done to demonstrate the substrate specificity of the RNF146 WWE domain. In addition, our data suggested that neither protein level nor PARylation levels of endogenous PARP1 was affected by overexpression of hRNF146 WWE domain. Second, the strength of PAR induction by the RNF146 WWE domain remains to be further tested. The level of PAR induction is comparable between PARG inhibition and WWE overexpression, yet the specific bands of PARylated proteins seem to be differed. Thus, these data indicated that either the RNF146 WWE domain was able to

increase the concentration for a particular subgroup of PARylated proteins or the preservation of cellular PAR levels was relatively inefficient compared to PARG inhibition. A systematic identification and analysis of individual PARylated proteins is needed in order to gain further insights into substrate specificity of RNF146 WWE domain. Stable isotope-labeled with amino acids in cell culture (SILAC), a method for quantitative proteomic analysis (Ong et al., 2002), would allow us to quantitatively identify which PARylated proteins are increased upon overexpression of RNF146 WWE domain. Meanwhile, additional mass-spectrometry analysis, using the RNF146 WWE domain as a bait to pull down endogenous PARylated proteins, can be utilized to further compare and validate the experimental results.

Bibiography

"Olaparib Approved for Advanced Ovarian Cancer." *Cancer Discovery* 5.3 (2015): 218.

Andrabi, Shaida A., et al. "Iduna Protects the Brain from Glutamate Excitotoxicity and Stroke by Interfering with Poly(ADP-Ribose) Polymer-Induced Cell Death." *Nature medicine* 17.6 (2011): 692-9.

Aravind, L. "The WWE Domain: A Common Interaction Module in Protein Ubiquitination and ADP Ribosylation." *Trends in biochemical sciences* 26.5: 273-5.

Ashworth, A. "A Synthetic Lethal Therapeutic Approach: Poly(ADP) Ribose Polymerase Inhibitors for the Treatment of Cancers Deficient in DNA Double-Strand Break Repair." *Journal of Clinical Oncology* 26.22 (2008): 3785.

Brown, Jessica,S., Stan Kaye B., and Timothy Yap A. "PARP Inhibitors: The Race is on." *British journal of cancer* 114.7 (2016): 713-5.

Caldecott, Keith W. "XRCC1 and DNA Strand Break Repair." *DNA Repair* 2.9 (2003): 955-69.

Callow, Marinella G., et al. "Ubiquitin Ligase RNF146 Regulates Tankyrase and Axin to Promote Wnt Signaling." *PLoS ONE* 6.7 (2011): e22595.

Chambon, P., J. D. Weill, and P. Mandel. "Nicotinamide Mononucleotide Activation of New DNA-Dependent Polyadenylic Acid Synthesizing Nuclear Enzyme." *Biochemical and biophysical research communications* 11 (1963): 39.

Chang, Paul, Myron K. Jacobson, and Timothy J. Mitchison. "Poly(ADP-Ribose) is Required for Spindle Assembly and Structure." *Nature* 432.7017 (2004): 645.

Dang, C. V., and W. M. Lee. "Identification of the Human c-Myc Protein Nuclear Translocation Signal." *Molecular and cellular biology* 8.10 (1988): 4048-54.

DaRosa, Paul A., et al. "Structural Insights into SAM Domain-Mediated Tankyrase Oligomerization." *Protein Science* (2016): n/a,n/a.

DaRosa, Paul A., et al. "Allosteric Activation of the RNF146 Ubiquitin Ligase by a Poly(ADP-Ribosyl)Ation Signal." *Nature* 517.7533 (2015): 223.

De Rycker, Manu, and Carolyn M. Price. "Tankyrase Polymerization is Controlled by its Sterile Alpha Motif and Poly(ADP-Ribose) Polymerase Domains." *Molecular and cellular biology* 24.22 (2004): 9802-12.

Di Girolamo, Maria, et al. "Physiological Relevance of the Endogenous Mono(ADP-Ribosyl)Ation of Cellular Proteins." *FEBS Journal* 272.18 (2005): 4565.

Fang, S., and A. M. Weissman. "Ubiquitin-Proteasome System." *Cellular and Molecular Life Sciences CMLS* 61.13 (2004): 1546-61.

Gao, Ying, et al. "Overexpression of RNF146 in Non-Small Cell Lung Cancer Enhances Proliferation and Invasion of Tumors through the Wnt/β-Catenin Signaling Pathway." *PLoS ONE* 9.1 (2013): e85377.

Haucke, Volker, et al. "The Yeast Mitochondrial Protein Import Receptor Mas20p Binds Precursor Proteins through Electrostatic Interaction with the Positively Charged Presequence." *Journal of Biological Chemistry* 270.10 (1995): 5565-70.

He, Fahu, et al. "Structural Insight into the Interaction of ADP-Ribose with the PARP WWE Domains." *FEBS letters* 586.21 (2012): 3858-64.

Hottiger, Michael O. "SnapShot: ADP-Ribosylation Signaling." *Molecular cell* 58.6: 1134,1134.e1.

Hu, Y., et al. "PARP1-Driven Poly-ADP-Ribosylation Regulates BRCA1 Function in Homologous Recombination-Mediated DNA Repair." *Cancer Discovery* 4.12 (2014): 1430.

Kalisch, Thomas, et al. "New Readers and Interpretations of Poly(ADP-Ribosyl)Ation." *Trends in biochemical sciences* 37.9: 381-90.

Kang, Ho Chul, et al. "Iduna is a Poly(ADP-Ribose) (PAR)-Dependent E3 Ubiquitin Ligase that Regulates DNA Damage." *Proceedings of the National Academy of Sciences of the United States of America* 108.34 (2011): 14103-8.

Kedersha, Nancy, et al. "Evidence that Ternary Complex (eIF2-GTP-tRNA(i)(Met))-Deficient Preinitiation Complexes are Core Constituents of Mammalian Stress Granules." *Molecular biology of the cell* 13.1 (2001): 195-210.

Kristeleit, R., et al. "2700 Final Results of ARIEL2 (Part 1): A Phase 2 Trial to Prospectively Identify Ovarian Cancer (OC) Responders to Rucaparib using Tumor Genetic Analysis." *European journal of cancer* 51: S531.

Langelier, M. F., and J. M. Pascal. "PARP-1 Mechanism for Coupling DNA Damage Detection to Poly(ADP-Ribose) Synthesis." *Current opinion in structural biology* 23.1 (2013): 134.

Leung, A. K., et al. "Poly(ADP-Ribose) Regulates Stress Responses and microRNA Activity in the Cytoplasm." *Molecular cell* 42.4 (2011): 489.

Leung, Anthony K. L. "Poly(ADP-Ribose): An Organizer of Cellular Architecture." *The Journal of cell biology* 205.5 (2014): 613-9.

Leung, Anthony K. L., et al. "Poly(ADP-Ribose) Regulates Post-Transcriptional Gene Regulation in the Cytoplasm." *RNA Biology* 9.5 (2012): 542-8.

Li, M., and X. Yu. "Function of BRCA1 in the DNA Damage Response is Mediated by ADP-Ribosylation." *Cancer Cell* 23.5 (2013): 693.

Li, Wei, and Yihong Ye. "Polyubiquitin Chains: Functions, Structures, and Mechanisms." *Cellular and molecular life sciences: CMLS* 65.15 (2008): 2397-406.

Martino-Echarri, Estefania, et al. "Tankyrase Inhibitors Stimulate the Ability of Tankyrases to Bind Axin and Drive Assembly of Î²-Catenin Degradation-Competent Axin Puncta." *PLoS ONE* 11.3 (2016): e0150484.

Mashimo, Masato, Jiro Kato, and Joel Moss. "Structure and Function of the ARH Family of ADP-Ribose-Acceptor Hydrolases." *DNA repair* 0 (2014): 88-94.

Messner, S., and M. O. Hottiger. "Histone ADP-Ribosylation in DNA Repair, Replication and Transcription." *Trends in cell biology* 21.9 (2011): 534.

Miwa, M., et al. "The Branching and Linear Portions of Poly(Adenosine Diphosphate Ribose) have the Same Alpha(1 Leads to 2) Ribose-Ribose Linkage." *Journal of Biological Chemistry* 256.6 (1981): 2916-21.

Niere, M., et al. "ADP-Ribosylhydrolase 3 (ARH3), Not Poly(ADP-Ribose) Glycohydrolase (PARG) Isoforms, is Responsible for Degradation of Mitochondrial Matrix-Associated Poly(ADP-Ribose)." *The Journal Of Biological Chemistry* 287.20 (2012): 16088.

Ong, Shao-En, et al. "Stable Isotope Labeling by Amino Acids in Cell Culture, SILAC, as a Simple and Accurate Approach to Expression Proteomics." *Molecular & Cellular Proteomics* 1.5 (2002): 376-86.

Plummer, R. "Poly(ADP-Ribose) Polymerase (PARP) Inhibitors: From Bench to Bedside." *Clinical oncology* 26.5: 250-6.

Ramamoorthy, Mahesh, and Susan Smith. "Loss of ATRX Suppresses Resolution of Telomere Cohesion to Control Recombination in ALT Cancer Cells." *Cancer Cell* 28.3: 357-69.

Rosenthal, Florian, et al. "Macrodomain-Containing Proteins are New Mono-ADP-Ribosylhydrolases." *Nat Struct Mol Biol* 20.4 (2013): 502-7.

Slade, Dea, et al. "The Structure and Catalytic Mechanism of a Poly(ADP-Ribose) Glycohydrolase." *Nature* 477.7366 (2011): 616.

Stowell, Alexandra I. J., et al. "A High-Throughput Screening-Compatible Homogeneous Time-Resolved Fluorescence Assay Measuring the Glycohydrolase Activity of Human Poly(ADP-Ribose) Glycohydrolase." *Analytical Biochemistry* 503 (2016): 58-64.

Vyas, Sejal, et al. "Family-Wide Analysis of Poly(ADP-Ribose) Polymerase Activity." *Nat Commun* 5 (2014).

Wang, Zhizhi, et al. "Recognition of the Iso-ADP-Ribose Moiety in Poly(ADP-Ribose) by WWE Domains Suggests a General Mechanism for Poly(ADP-Ribosyl)Ation-Dependent Ubiquitination." *Genes & development* 26.3 (2011): 235-40.

Welchman, Rebecca L., Colin Gordon, and R. J. Mayer. "Ubiquitin and Ubiquitin-Like Proteins as Multifunctional Signals." *Nature reviews. Molecular cell biology* 6.8 (2005): 599-609.

Wen, Wei, et al. "Identification of a Signal for Rapid Export of Proteins from the Nucleus." *Cell* 82.3: 463-73.

Wenzel, Dawn M, Kate E Stoll, and Rachel E Klevit. "E2s: Structurally Economical and Functionally Replete." *Biochemical Journal* 433.1 (2011): 31-42.

Ye, Yihong, and Michael Rape. "Building Ubiquitin Chains: E2 Enzymes at Work." *Nature reviews. Molecular cell biology* 10.11 (2009): 755-64.

Zahradka, Peter, and Kaney Ebisuzaki. "A Shuttle Mechanism for DNA-Protein Interactions." *European Journal of Biochemistry* 127.3 (1982): 579.

Zhang, Yue, et al. "RNF146 is a Poly(ADP-Ribose)-Directed E3 Ligase that Regulates Axin Degradation and Wnt Signalling." *Nature cell biology* 13.5 (2011): 623.

Curriculum Vitae

Haobo Wang

haobo1221@gmail.com

667-214-6700

Education

Shanghai University (2008-10)

Major: Bioengineering

Scholarship for New Incoming Freshman (2008-09)

University of Oregon (2010-2014)

Degree: Bachelor of Science

Major: Biochemistry

Minor: Biology

The Johns Hopkins University Bloomberg School of Public Health (2014 - present)

Master of Science at Department of Biochemistry and Molecular Biology (2014 - 2016)

Doctor of Philosophy at Department of Biochemistry and Molecular Biology (2016 - 2021)

Undergraduate Experience

- Worked in biology research lab on neural cell expression under graduate student in Shanghai University for 6 months (March - August, 2010);
- Transferred to University of Oregon in September, 2010;
- Participated in research project under Dr. Diane Hawley on regulation mechanism for the eukaryotic

transcription of RNA polymerase II in *Saccharomyces cerevisiae* at University of Oregon since June, 2012;

- Teaching assistant for General Chemistry lab CH227 from September, 2012 - December, 2012;
- Teaching assistant for Organic Chemistry lab CH338 from January, 2013 - March, 2013;
- Undergraduate Research Report at University of Oregon:

  Phenotypical Examination of Mutations in RNA Polymerase II And Transcription Factors That Affect Elongation Process In *Saccharomyces cerevisiae*.

- Graduated from University of Oregon in June, 2014;

Graduate School Experience

- Worked in Dr. Anthony Leung' s lab on ADP-ribosylation and WWE domain
- First year thesis:

  A Novel Signaling Network Shared by Post-translational Modification Mediates DNA Double-Strand Break Repair Response Through Its Regulations of BRCA1-Containg Repair Complexes in Both Normal and *BRCA1*- deficient Breast Cancer Cells

- ScM thesis:

  Characterization and Application of Ubiquitin E3 Ligase RNF146 WWE Domain